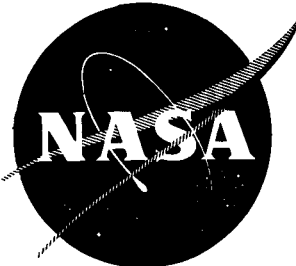


NASA CR-72169

~~DIT Report~~-160-9 END



ANALYTICAL STUDY
OF THE FRACTURE OF LIQUID-FILLED TANKS
IMPACTED BY HYPERVELOCITY PARTICLES

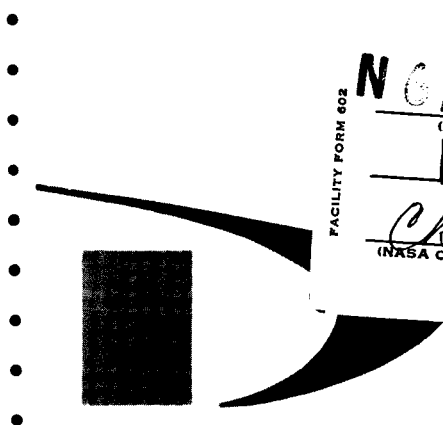
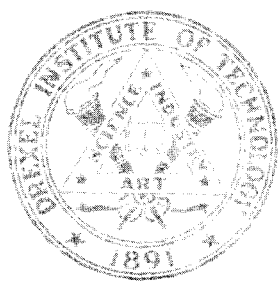
by

Pei Chi Chou
Richard Schaller
James Hoburg

Prepared for
NATIONAL AERONAUTICS AND SPACE ADMINISTRATION
Lewis Research Center

MARCH 1967

NASA Contract NsG-270



FACILITY FORM 602

N 67-22068
(ACCESSION NUMBER)

10 74 RS 22-26
(PAGES)

CR-72169
(NASA CR OR TMX OR AD NUMBER)

(THRU) _____

(CODE) **1**

(CATEGORY) **32**

NOTICE

This report was prepared as an account of Government sponsored work. Neither the United States, nor the National Aeronautics and Space Administration (NASA), nor any person acting on behalf of NASA:

- A) Makes any warranty or representation, expressed or implied, with respect to the accuracy, completeness, or usefulness of the information contained in this report, or that the use of any information, apparatus, method, or process disclosed in this report may not infringe privately owned rights; or
- B) Assumes any liabilities with respect to the use of, or for damages resulting from the use of any information, apparatus, method or process disclosed in this report.

As used above, "person acting on behalf of NASA" includes any employee or contractor of NASA, or employee of such contractor, to the extent that such employee or contractor of NASA, or employee of such contractor prepares, disseminates, or provides access to, any information pursuant to his employment or contract with NASA, or his employment with such contractor.

Requests for copies of this report should be referred to:

National Aeronautics and Space Administration
Office of Scientific and Technical Information
Attention: AFSS-A
Washington, D.C. 20546

1134

3 ANALYTICAL STUDY
OF THE FRACTURE OF LIQUID-FILLED TANKS
IMPACTED BY HYPERVELOCITY PARTICLES 6

by
6 Pei Chi Chou
Richard Schaller
James Hoburg 9

Prepared for
NATIONAL AERONAUTICS AND SPACE ADMINISTRATION
Lewis Research Center

9 MARCH 1967 10CV

26 Grant ~~Contract~~ NSG-270 29A

Technical Management
NASA Lewis Research Center
Chemical Rocket Division
Cleveland, Ohio
Richard N. Johnson

1 Drexel Institute of Technology
32nd and Chestnut Streets
Philadelphia, Pennsylvania 19150 3

TABLE OF CONTENTS

ABSTRACT.iv
SYMBOLSv
SUMMARY1
I. INTRODUCTION2
II. SHOCK WAVES IN WATER.5
III. STRESS WAVES IN TANK WALLS.9
IV. THRESHOLD IMPACT ENERGY16
V. PARAMETRIC CALCULATIONS AND FRACTURE KINETIC ENERGY18
VI. CONCLUDING REMARKS.22
VII. FIGURES23

APPENDICES

A. Approximate Treatment of the Jump Conditions.43
B. Computer Program for Numerical Calculations47

LIST OF FIGURES

Page No.

1. Comparison of the exact and approximate shock front positions, shock radius versus time, K.E. = 140 ft-lbs, $r_0 = 7/64$ in.23

2. Comparison of the exact and approximate peak pressures as functions of radius, K.E. = 140 ft-lbs, $r_0 = 7/64$ in.24

3. Pressure distribution behind the shock front in water due to impact.. . .25

4. Values of the pressure at grid points during early time after impact. . . .26

5. Characteristic network for application of numerical procedure.27

6. Comparison of the response of a plate, M_θ versus time at $r = r_0$, for three different mesh sizes, under a projectile kinetic energy input of 140 ft-lb, $r_0 = 7/64$ in., $h = 1/32$ in.28

7. Response of a 7075-T6 aluminum plate at several radii under an impact kinetic energy of 140 ft-lb, $r_0 = 7/64$ in., $h = 1/32$ in.

 a. Moment M_θ versus time.29

 b. Moment M_r versus time.30

 c. Shear force Q_r versus time.31

 d. Transverse velocity of the plate w_t versus time.32

 e. Transverse displacement of the plate w versus time.33

8. Transverse plate displacement versus radius, for a 1/64 in. thick 7075-T6 aluminum plate under a projectile kinetic energy of 50 ft-lb.. . .34

9. Threshold kinetic energy versus plate thickness for 7075-T6 aluminum with an inner radius $r_0 = 7/64$ in.35

10. Threshold kinetic energy versus plate thickness for 5AL-2.5 Sn (ELI) titanium with an inner radius $r_0 = 7/64$ in.36

11. Threshold kinetic energy versus plate inner radius for 7075-T6
aluminum with a constant plate thickness, $h = 1/32$ in.37

12. Comparison of "exact" numerical solution and approximate solution
neglecting jump conditions.38

13. Comparison of "exact" numerical solution and approximate solution
neglecting jump conditions for a Timoshenko beam.39

TABLE I 21

ABSTRACT

The problem of the fracture of liquid-fuel tank walls due to hypervelocity particle impact is investigated. A semi-empirical formula is used for the shock wave generated by impact in water. The numerical method of characteristics is adopted for the calculation of stress waves in the tank wall. Values of threshold impact kinetic energy, defined as the projectile energy above which fracture will occur, for a few wall thickness and materials are determined.

SYMBOLS

a, b, c	=	constants
c_p	=	plate velocity = $[E/\rho(1-\nu^2)]^{1/2}$
c_2	=	shear wave velocity = $(G/\rho)^{1/2}$
D	=	flexural rigidity = $Eh^3/12(1-\nu^2)$
E	=	modulus of elasticity
$F(r, t)$	=	surface traction, function of radial distance and time (force/unit area)
G	=	shear modulus = $E/2(1+\nu)$
h	=	plate thickness
K	=	constant
k_2^2	=	shear correction factor
KE	=	kinetic energy of the impacting projectile
M_r	=	radial bending moment
M_θ	=	tangential bending moment
P_0	=	pressure in water ahead of shock front
P_1	=	peak pressure behind shock front
Q_r	=	transverse shear stress resultant
R	=	shock front radius
r	=	radial distance
r_0	=	inner radius of plate
t	=	time
U	=	shock front velocity
u	=	particle velocity in water

- w = transverse displacement of the midplane
- γ = constant
- θ = tangential direction
- ν = Poisson's ratio
- ρ = density of plate
- ρ_0 = density of water ahead of shock front
- ρ_1 = density of water behind shock front
- σ = normal stress due to M_θ
- τ = shear stress due to Q_r
- ϕ = rotation of the cross-section about the tangential axis

Subscripts r and t designate partial differentiations
(except Q_r and M_r).

ANALYTICAL STUDY OF THE FRACTURE OF LIQUID-FILLED TANKS IMPACTED BY
HYPERVELOCITY PARTICLES

by

Pei Chi Chou, Richard Schaller, and James Hoburg

SUMMARY

This is a report on a study of the problem of the fracture of liquid-fuel tanks due to hypervelocity particle impact. The impact generates a shock wave in the liquid fuel. Calculations for the response of tank walls which are initially prepunched, i.e., have a hole at the center, and subjected to an axisymmetric moving shock wave are made. For simplicity, the liquid behind the tank wall is assumed to be water. Calculations for the magnitude of the pressure distribution behind the shock are made, utilizing the shock Hugoniot data for water, along with a semi-empirical formula relating the position of the shock front as a function of time and impacting kinetic energy.

Values of impact kinetic energies that produced a stress equal to the dynamic fracture strength of the material, assumed to be twice the value of the static yield strength, are found for 7075-T6 aluminum and 5AL-2.5 Sn titanium alloy tank walls with various hole sizes and thicknesses.

For the case of unpunched walls an estimation is made of the kinetic energy absorbed by the wall during perforation. A correlation is then made between the experimental energy necessary to produce fracture and the calculated energy necessary to produce fracture, (i.e. the sum of the threshold and perforation energies), for several unpunched walls under various impact conditions. The results are found to be in general agreement.

I INTRODUCTION

This report deals with the catastrophic failure (fracture) of a liquid-fuel tank wall due to hypervelocity particle impact. This particle may be an uninterrupted meteoroid, or from the debris of the protective thin bumper after being impacted by a high speed meteoroid.

The process from the moment of impact to the final failure of the tank wall may be generally divided into three stages, namely, the initial perforation, or puncture, the subsequent shock wave produced in the liquid fuel, and the final motion and fracture of the wall.

The perforation of thin plates by hypervelocity particles has been studied recently by many investigators. Bull (Ref. 1) assumed a one-dimensional compressible-fluid model and performed both theoretical and experimental studies. Chou (Ref. 2 and 3) and Kraus (Ref. 4) assumed a visco-plastic model and a perforation criterion, from which the critical impact velocity and mass of the projectile may be calculated. Recently, this visco-plastic model has been verified by Kruszewski of NASA Langley Research Center, (Ref. 5). Other perforation studies have been carried out by Watson (Ref. 6), and Maiden and McMillan (Ref. 7). All of these perforation studies are for thin plates without liquid behind them. Very little information is available for the perforation of plates with water or other liquid behind them. Stepka and Morse (Refs. 8 and 9) made experimental investigation of the overall problem of impact fracture of fuel tanks; they did not investigate in particular the perforation phase of the problem.

Shock waves produced in liquids due to high speed particle impacts have been measured by Stepka, Morse, and Dengler (Ref. 10), and also Ferguson (Ref. 11). Stepka, et al, made extensive measurement of the shock waves produced in water, while Ferguson made limited measurements of shocks in liquid hydrogen. Presented in Reference 12 is a semi-empirical formula for the shock front radius and velocity, which agrees fairly well with the experimental results in both References 10 and 11. Because of the uncertainty of the shock Hugoniot data, the pressure behind the shock front cannot be calculated accurately for liquid hydrogen. For this reason, the present report will be limited to discussion on water filled tanks only. The technique presented here may be applied to any liquid as long as its shock Hugoniot data is known. The semi-empirical formula of Reference 12, which is based on the kinetic energy of the projectile, will be used in this report for calculating the shock radius in water.

It will be shown that the maximum stress in the tank wall is due to bending created by the shock wave in liquid, and occurs a few microseconds after impact. In Reference 13, a numerical method of characteristics was presented for the calculation of bending waves in plates due to stationary concentrated ring loads applied at the edge of the plate. In this report, the method of Reference 13 is extended to include the moving load of the traveling shock wave. It is found that the maximum stress always occurs at the edge of the perforated hole of the wall. After the maximum stress is calculated, a failure criterion is adopted, which stipulates that the wall will crack if the maximum stress is larger than twice the static yield stress of the wall material. In other words, the dynamic strength is assumed to be twice the static yield stress. Once a crack occurred, the additional pushing from the high pressure region in water should keep it propagating to complete failure.

Combining the shock wave formulas, the stress wave in tank wall calculation, and the failure criterion, a threshold impact energy is established for a plate of given material, thickness, and hole diameter (approximately the projectile diameter). For impacts with kinetic energies entering water above the threshold value, fracture will occur. A parametric calculation of the threshold kinetic energy as functions of wall plate thickness and projectile diameter for 7075-T6 aluminum and 5AL-2.5 Sn titanium alloy was made and results presented in this report.

In order to compare the present calculated results with the experimental results of References 8 and 9, an estimation of the energy required for the initial perforation is made. Values of the sum of the perforation energy and the threshold energy are in general agreement with the kinetic energies of projectiles that actually perforated and burst the tanks.

Two appendices are included: the first one gives justification of some of the assumptions used in the stress wave calculation, the second appendix contains the basic computer program for the calculations of this report.

II SHOCK WAVES IN WATER

A. Shock Front and Peak Pressure

The high pressure region created in water after being impacted by a high velocity projectile has been studied in Refs. 10 and 12. In Ref. 12 a simple semi-empirical equation is presented which gives the shock radius and peak pressure as functions of time. The experimental results reported in Ref. 10 are in agreement with this equation. In this report, the semi-empirical equation of Ref. 12 will be utilized.

The equations for the shock radius, R, and shock velocity, U, as derived in Ref. 12, are

$$R = 0.05678t + 0.0197 (K E)^{1/3} \log_e(t + 1) \quad (1)$$

$$U = \frac{dR}{dt} = 0.05678 + \frac{0.0197 (K E)^{1/3}}{t + 1} \quad (2)$$

where R is in inches, t in microseconds, kinetic energy in ft-lbs, and U in inches per usec. As can be seen, eqs. 1 and 2 are based on the assumption that the shock wave in water depends only on the kinetic energy of the projectile, and is independent of other properties of the projectile. The particle velocity, u, may be calculated from U once the shock Hugoniot is known. We shall use the semi-empirical shock Hugoniot relation for water presented by Rice and Walsh (Ref. 14).

$$U = 1.483 + 25.306 \log_{10} \left(1 + \frac{u}{5.19} \right) \quad (3)$$

Where u and U are expressed in Km/sec.

From the conservation of mass and momentum across the shock front, the following simple equations may be obtained.

$$u = \frac{\rho_1 - \rho_0}{\rho_1} U \quad (4)$$

$$U = \left[\left(\frac{\rho_1}{\rho_0} \right) \frac{P_1 - P_0}{\rho_1 - \rho_0} \right]^{1/2} \quad (5)$$

where P is pressure in psi, ρ is density in $\frac{\text{lbf-}\mu\text{sec}^2}{\text{in}^4}$ and subscripts

1 and 0 refer to properties behind and ahead of the shock, respectively.

Substituting eq. (4) into eq. (5) and rearranging we obtain

$$P_1 = Uu \rho_0 + P_0 \quad (6)$$

For a given impact kinetic energy, U may be calculated from (1) and (2) as a function of R; then u can be calculated from (3); and P_1 as a function of R from (6).

B. Approximate Shock Front and Peak Pressure

For convenience in computer calculation, the shock radius vs. time curve as given by eq. (1) is approximated by two straight lines in the $r, c_p t$ -plane. The equations of these two straight lines are

$$\begin{aligned} c_p t - ar &= 0 \\ c_p t - br &= c \end{aligned} \quad (7)$$

A comparison of the curve given by eq. (1) with the corresponding curves by (7) is shown in Figure 1, which is for an impacting particle with a 7/32 in. diameter and an impact K.E. of 140 ft-lbs. In this case, for a 7075-T6 aluminum plate the value of $c_p = 2.10334 \times 10^5$ in/sec. and the values of a, b and c are

$$a = 1.8476$$

$$b = 2.8889$$

$$c = 0.5978$$

The peak pressure vs. shock radius curve, as calculated from eqs. (1), (2), (3), and (6), is likewise approximated by a simple equation for easy computer application. This equation is of the form

$$P_1 = KR^Y \quad (8)$$

Figure 2 shows, for a 140 ft-lbs impact, the curve of eq. (8) as compared to the one from eq. (6). In this case $K = 2.0656 \times 10^4$, $\gamma = -1.65$. The value of one of the constants, K or γ , is determined by the condition that the value of P_1 from eq. (8) is exact at $r = r_0$. The other constant is fixed by the simple inspection of curves plotted from various values of this constant.

C. Pressure Distribution Behind the Shock Front

The pressure in water between the shock front and the edge of the hole is acting on the tank wall, in addition to the peak pressure at the shock front. The exact distribution of this pressure is not known precisely, although Stepka and Morse (Ref. 8) have made some preliminary experimental measurements. Their experiment consisted essentially of placing two pressure sensing devices in water at distances of 1.44 in. and 1.87 in., respectively, from the point of impact. The measured pressure vs. time curves shown in Figure 9 of Ref. 8 contain considerable oscillations. However, if the oscillations are ignored, the average values of each of these curves may be used to estimate the pressure distribution behind the shock front.

It is reasonable to assume that at the edge of the plate, $r = r_0$, the pressure is zero, or, atmospheric, which for our practical purposes may be considered zero. We shall further assume that the pressure behind the shock front varies according to the fourth power of the radius measured from r_0 ; this may be expressed as

$$\frac{P}{P_1} = \left(\frac{r - r_0}{R - r_0} \right)^4 \quad (9)$$

Figure 3 shows a plot of this equation, together with a few experimental points as obtained by Stepka and Morse in Ref. 8. In plotting

these points, eq. (1) is used for the position of the shock front, and the value of r_0 is 7/64 in. As can be seen, equation (9) agrees fairly well with the test data.

In the numerical calculation, a constant pressure distribution behind the shock front is assumed for early times after impact, up to one usec. This assumption was introduced because of the limited number of grid points in the r, c_p, t plane (physical plane) during the early times. Within a short time after impact, the peak pressure decays quite rapidly along the shock front, this, coupled with the rapid decay behind the shock, causes a very large difference in values of pressures at two neighboring points in the physical plane. For example, for a kinetic energy of 140 ft-lbs., the pressures at the first few points in the physical plane are shown in Figure 4 for a mesh size of $\Delta r = 0.00625$ in. Along the constant time lines where there are only one or two points with pressure different from zero, the total force on the plate is much higher than it should be. For example, along one constant time line (ABD) there is only one grid point to the left of the shock, at this grid point; B, the pressure is 100,000 psi. Within the finite-difference scheme of calculation, this is equivalent to assuming that this pressure is uniformly distributed from the shock front to the boundary, $r = r_0$, i.e. A to D. The total force, eg. $100,000 \pi(r_D^2 - r_0^2)$, acting in such a case is much higher than that produced by equation (9) at this time. Furthermore, this total force at a given time varies with the mesh size used in the numerical calculation.

To remedy this situation, a constant pressure distribution is assumed for time less than one usec. Along each constant time line, a constant pressure of one-fifth that at the shock front is used. The

total force acting on the plate due to this constant pressure is approximately the same as that due to the actual pressure distribution of equation (9) at any particular time.

After one μsec , the pressures no longer vary drastically from point to point, the total force is no longer highly dependent upon mesh size, and there are more grid points along each constant time line. Thus, after this time, we use the true pressure distribution as given by eq. (9).

III STRESS WAVES IN TANK WALLS

A. Characteristic Equations

The Uflyand-Mindlin equations, in polar coordinates, for an elastic plate with surface tractions under axisymmetrical loading conditions are:

$$\frac{\partial M_r}{\partial r} + \frac{1}{r} (M_r - M_\theta) - Q_r = \frac{\rho h^3}{12} \frac{\partial^2 \theta}{\partial t^2} \quad (10)$$

$$\frac{\partial Q_r}{\partial r} + \frac{1}{r} Q_r + F(r,t) = \rho h \frac{\partial^2 w}{\partial t^2} \quad (11)$$

$$M_r = D \left(\frac{\partial \phi}{\partial r} + \frac{\nu}{r} \phi \right) \quad (12)$$

$$M_\theta = D \left(\frac{\phi}{r} + \nu \frac{\partial \phi}{\partial r} \right) \quad (13)$$

$$Q_r = K_2^2 G h \left(\phi + \frac{\partial w}{\partial r} \right) \quad (14)$$

Due to the axisymmetrical loading conditions, it is evident that $M_{r\theta} = Q_\theta = \frac{\partial}{\partial \theta} = 0$. Equations (10), (12), (13), and (14) are identical to equations (1), (3), (4), and (5) of Ref. 13. Equation (11) differs from equation (2) of Ref. 13 in that it has an added surface traction term $F(r,t)$. The system of equations (10) to (14) are hyperbolic

equations and their characteristic directions and characteristic equations have been derived by Jahsman in Ref. 15. In this report, we shall follow the displacement approach which uses a system of two second-order equations involving ϕ and w . The method of characteristics is applied to this set of second-order equations. Substituting eqs. (12), (13), and (14) into eqs. (10) and (11) we have

$$\frac{\partial^2 \phi}{\partial r^2} - \frac{\rho h^3}{12D} \frac{\partial^2 \phi}{\partial t^2} = \frac{k_2^2 Gh}{D} \left(\phi + \frac{\partial w}{\partial r} \right) + \frac{1}{r^2} \phi - \frac{1}{r} \frac{\partial \phi}{\partial r} \quad (15)$$

$$\frac{\partial^2 w}{\partial r^2} - \frac{\rho}{k_2^2 G} \frac{\partial^2 w}{\partial t^2} = -\frac{1}{r} \left(\phi + \frac{\partial w}{\partial r} \right) - \frac{\partial \phi}{\partial r} - \frac{F(r,t)}{k_2^2 Gh} \quad (16)$$

Equations (15) and (16) are also hyperbolic in nature and their physical characteristics, or characteristic directions, are, as demonstrated in Ref. 13,

$$\left. \begin{array}{l} I^+ \\ I^- \end{array} \right\} \frac{dr}{dt} = \pm c_p \quad (17)$$

$$\left. \begin{array}{l} II^+ \\ II^- \end{array} \right\} \frac{dr}{dt} = \pm k_2 c_2 \quad (18)$$

Equations (17) and (18) represent four physical characteristics. For a plate in which E , ρ , and ν are constant, the two wave speeds, as given by eqs. (17) and (18) are constant, and the physical characteristics are straight lines when represented in the $r, c_p t$ -plane.

The characteristic equations along I^+ and I^- are, respectively,

$$\frac{1}{c_p} d\phi_t \mp d\phi_r = \mp \left(\frac{k_2^2 Gh}{D} \left(\phi + w_r \right) + \frac{\phi}{r^2} - \frac{\phi_r}{r} \right) dr \quad (19)$$

where the upper signs refer to I^+ , and the lower signs to I^- . The

characteristic equations along II^+ and II^- respectively.

$$dw_r \mp \frac{1}{k_2 c_2} dw_t = - \left(\frac{1}{r} (\phi + w_r) + \phi_r + \frac{F(r,t)}{k_2^2 Gh} \right) dr \quad (20)$$

Again, we see that equation (20) differs from equation (11) of Ref. 13 by an added surface traction term, $F(r,t)$, which is a known function. These four equations, (19) and (20) govern the variation of the variables w_r , w_t , ϕ_r , and ϕ_t , along the physical characteristic directions. Two additional equations, based on the continuity of ϕ and w , or

$$d\phi = \phi_r dr + \phi_t dt \quad (21)$$

$$dw = w_r dr + w_t dt \quad (22)$$

can be written along any direction. For instance, along a vertical direction $dr = 0$, (21) and (22) may be written as

$$d\phi = \phi_t dt \quad (23)$$

$$dw = w_t dt \quad (24)$$

We now have a system of six equations (19), (20), (21), and (22)

for the six variables w_r , w_t , ϕ_r , ϕ_t , ϕ , and w .

B. Initial and Boundary Conditions

The problem treated in this report involves an infinite plate with a circular hole of radius r_0 . Thus, the region is specified by $r_0 \leq r < \infty$. The proper initial conditions for this problem require the specification of the four variables ϕ_r , ϕ_t , w_r , and w_t at $t = 0$. For the case of our infinite plate under no initial loads and velocity, the initial conditions are

$$\phi_r(r,0) = \phi_t(r,0) = w_r(r,0) = w_t(r,0) = 0, \quad r_0 \leq r < \infty. \quad (25)$$

At $r = r_0$, a properly posed boundary condition requires the specification of one of the two functions ϕ_r and ϕ_t , and one of the two functions w_r and w_t . Or, alternatively, by using equations (12), (13), and (14), any two of the five functions M_r , M_ϕ , Q_r , ϕ_t , and w_t may be specified along $r = r_0$. For the present fuel tank problem the proper boundary conditions are

$$Q_r \equiv M_r \equiv 0 \text{ at } r = r_0 \quad (26)$$

As discussed before, the moving load on the tank wall will be due to a spherical hydrodynamic shock wave that travels through the fuel after impact. The position, velocity, and pressure of the shock front as well as the pressure distribution behind it have been discussed in Section II.

Since the wave front travels along a line specified by equation (1) or (7), the region between this line and $t = 0$ in the physical plane (r vs. $c_p t$) is free of surface tractions. Therefore, this region contains the trivial solution of vanishing derivatives of ϕ and w .

In Ref. 13 the problem of discontinuities in the first derivatives of displacement due to step or jump inputs at the boundary was treated. With a step input in stress, moment, or particle velocity at the boundary, discontinuities in stress, moments, or the first derivatives of displacement could exist across the two right running physical characteristics (eqs. (17 and (18), with the upper sign) emitted from the mesh point $r = r_0$ at $t = 0$.

For the present problem the peak pressure front of the moving load is actually a discontinuous surface traction (step input) moving out

over the plate. This means that discontinuities (jumps) in the first derivatives of ϕ and w could occur along all physical characteristics emanating from the shock front line in the physical plane. This condition would make the problem extremely difficult to solve from the numerical standpoint.

To eliminate the condition of lines of possible discontinuities in the physical plane, jump conditions were simply neglected. Justification for this approach is given in Appendix A.

C. Numerical Procedures

The procedure for numerical calculations is adapted from that presented in Ref. 13. Evenly spaced I^+ and I^- characteristics are used as the main network as shown in Figure 5. Although there are four families of characteristic lines in the physical plane, only properties at the grid points, the intersections of I^+ and I^- characteristics, will be calculated. The values at points 5 and 6 of Figure 5 which lie along II^+ and II^- characteristics are found by linear interpolation. For example, the values at point 5 are found by linear interpolation between those at points 2 and 4. Therefore, assuming that the values of the variables at the back points 2, 3, 4, 5 and 6 are known we can now write eqs. (19), (20) (with the upper and lower signs along the corresponding characteristics), (21) and (22) in finite difference form. This gives us six equations to solve for the six unknowns ϕ , ϕ_r , ϕ_t , w , w_r , and w_t at point 1.

For points on the boundary $r = r_0$, the I^+ and II^+ characteristics represented by eqs. (19) and (20) with the upper signs are absent. For

this problem, M_r and Q_r are specified along $r = r_0$. Therefore, eqs. (12) and (14) along with eqs. (19), (20) (with the lower signs), (21), and (22) form a system of six equations necessary for the determination of the six variables ϕ , ϕ_r , ϕ_t , w , w_r , and w_t .

D. Specific Example

The problem considered in detail involved a plate made of 7075-T6 aluminum with the following dimensions and elastic properties:

$$\begin{aligned}\rho &= 0.2613 \times 10^{-3} \text{ lb-sec}^2/\text{in} & k_2^2 &= 0.85 \\ G &= 3.9 \times 10^6 \text{ lb/in}^2 & E &= 10.4 \times 10^6 \text{ lb/in}^2 \\ r_0 &= 7/64 \text{ in.} & \nu &= 0.33 \\ h &= 1/32 \text{ in.}\end{aligned}$$

This plate is of the same dimension and material as one in the experimental tests made on plates with prepunched holes by Stepka and Morse, as presented in Table 1 of Ref. 8. The projectile had a mass of 0.042 lbm/cu.in. and a velocity of 6300 ft/sec. which gave an impact kinetic energy of 140 ft-lbs.

The calculations were performed on an IBM 7040 computer, with an average running time of 30 minutes to obtain a plate response history of 20 μ sec. For the assumed pressure distribution discussed in Section II, it was found that the solutions converged to a stable value when a mesh size of $\Delta r = 0.00625$ was used. Figure 6 shows a plot of M_θ (the bending moment in the θ -direction) versus time at the boundary ($r = r_0$) for three different mesh sizes, $\Delta r = .0125$, $.00625$ and $.003125$. As can be seen, the difference between the curves with the two smaller mesh sizes is very slight. It was also found that the same order of magnitude of difference existed for all the dependent variables, both at the boundary and at interior points in the plate.

Figures 7a through 7e show the distribution M_{θ} , M_r , Q_r , w (plate deflection), and w_t (plate velocity) at several radii.

The maximum bending moment generated in the plate occurred at the boundary ($r = r_0$). This can be observed by comparing values of M_{θ} and M_r at several radii in Figures 7a and 7b to the values of M_{θ} at the boundary ($r_0 = 7/64$ in.) in Figure 6. The maximum normal stress generated in the plate due to bending can be obtained from the following formula (see Ref. 16).

$$\sigma_{\theta} = \frac{6M_{\theta}}{h^2} \quad (27)$$

We see from Figure 6 that M_{θ} reaches a maximum of 24.75 in-lb/in. in 1.66 μ sec. Therefore the bending stress for this impact reaches a maximum value of 152,000 psi in the same time interval.

The shear stress at any point in the plate is given by (Ref. 17).

$$\tau = \frac{3}{2} \frac{Q_r}{h} \quad (28)$$

We see from Figure 7c that Q_r (transverse shear stress resultant) builds up to a maximum value of -800 lb/in. at $r = 0.25$ inch within 1.4 μ sec. Substituting this value of Q_r into eq. (28) gives a value for the maximum shear stress of 40,000 psi, which is about one-fourth the value of the maximum bending stress. From other impact conditions it was also observed that the maximum value of the shear stress did not become much larger than one-fourth of the maximum value of the normal stress in the plate. Therefore it can be concluded that the stress governing failure is the bending stress obtained from eq. (27).

IV THRESHOLD IMPACT ENERGY

Rinehart and Pearson in Ref. 18 have listed experimental values of the critical normal fracture stress for several metals under the action of dynamic or impulsive loads. Their results indicate that the dynamic fracture stress of a metal under dynamic loading conditions is approximately twice the value of the static yield strength of the metal.

We shall define a threshold impact energy as the kinetic energy that will create, in a plate, a bending stress twice the value of the static yield stress of the material. Therefore, any kinetic energy less than the threshold kinetic energy is a safe value.

For 7075-T6 aluminum the static yield strength is 77,000 psi, therefore the dynamic fracture stress of this metal would be 154,000 psi. It was found in the previous section that a projectile kinetic energy of 140 ft-lb. generated a bending stress of 152,000 psi in a 1/32 in. thick 7075-T6 aluminum plate with an inner radius of $r_o = 7/64$ in. Calculations made for the same plate thickness and the same projectile diameter, but at a higher impact velocity corresponding to an impact kinetic energy of 210 ft-lbs., yielded a maximum bending stress of 194,000 psi, considerably higher than the dynamic fracture stress. By interpolation, the threshold kinetic energy of 143 ft-lb. is obtained for this plate. Experimental results reported in Ref. 8 indicated that a kinetic energy of 210 ft-lb. failed a 1/32 in. plate, whereas a kinetic energy of 140 ft-lb. did not fail the plate; in agreement with our calculation.

In all cases that we considered in this report, the plates were assumed to be prepunched, therefore all the kinetic energy of the

projectile was transferred into the water behind the plate. Stepka and Morse only stated results for one prepunched plate which was for 7075-T6 aluminum with a plate thickness of 1/32 of an inch, see Table I of Ref. 8. This case gave good correlation with the results found in this report as was previously pointed out. In order to compare the results of this report with the rest of the tests in References 8 and 9, which are for unpunched plates, we must now consider the amount of projectile kinetic energy that is necessary to puncture the plate.

In an unpunctured plate there is a partition of the impact energy into the amount necessary to puncture the plate and the remaining amount that creates a high pressure region in the water. A comparison of the threshold kinetic energy as obtained in this report with the experimental values of References 8 and 9 will be pointed out in the following section.

In the analysis of the moving load problem the linear plate equations (10) to (14) were used. These basic equations are only valid under the conditions of small deflections. If large deflections occur in the plate then the non-linear Von Karman equations or the membrane equations must be used to describe the plate behavior, as was done in Ref. 19.

It was found that for a 1/64 in. thick 7075-T6 aluminum plate, which was the thinnest plate studied, the maximum plate deflection did not exceed 0.017 inches for a kinetic energy of 50 ft-lb, which is the threshold kinetic energy for the plate. Figure 8 shows a plot of the transverse displacement of the midplane of the plate, w , versus r at the time when the maximum bending moment M_0 , and the maximum bending stress occur in the plate. At this time, the wave front in the plate is at a radius of 0.48 inches. Since 0.017 inches is not a large deflection for a plate radius of 0.48 inch, it can be concluded that the linear plate equations sufficiently described the behavior of the plates for the present case.

V PARAMETRIC CALCULATIONS AND FRACTURE KINETIC ENERGY

The stresses generated in a plate subjected to a moving load depend upon the material used, i.e., E , G , ν , and ρ , and the geometry of the plate, in this case the inner radius r_0 and the plate thickness h . Therefore, if we consider the problem of a particle with a given kinetic energy impacting into water through a hole in a plate, the stresses generated in the plate due to the high pressure in the water may vary considerably if the geometry or the material of the plate is changed.

Included in this report is a parametric study of two materials, 7075-T6 aluminum and 5AL-2.5 Sn (ELI) titanium alloy. The first material was studied because there is sufficient experimental data available in references 8 and 9 for comparison purposes. The second metal was chosen because of its potential use in the application of liquid fuel tanks.

Figures (9) and (10) are plots of threshold kinetic energy versus plate thickness for the two different materials, both with $r_0 = 7/64$ in. Note that as the plate thickness is increased, a higher impacting kinetic energy is needed to fail the plate. This is because the resistance due to bending increases as the plate thickness increases. It was previously pointed out that the critical stresses generated in the plate were the normal stresses due to bending, therefore it takes a higher impacting kinetic energy to generate the same critical bending stress σ_0 in a thicker plate. It should be noted that the points on these curves are computer calculated, not experimental data.

Figure (11) is a plot of the threshold kinetic energy versus the plate inner radius r_0 for a $1/32$ in. thick 7075-T6 aluminum plate. It is interesting to note that for the same kinetic energy input if the inner radius of the plate is allowed to decrease, the bending moment M_0 at the boundary $r = r_0$ increases. Hence, it takes a smaller threshold kinetic energy to fail

a given plate with a smaller inner radius. This fact is illustrated in Figure (11) of this report and also in Table I of Reference 9, assuming that the given projectile radius is equal to r_0 .

The threshold kinetic energies which are obtained in this report for a 1/32 in. thick 7075-T6 aluminum plate with different inner radii are consistently lower than those presented in Reference 9. The reason, as was pointed out earlier in this report, is that in our calculation the impacting particle is assumed to deliver all of its kinetic energy to the water behind the plate. This condition is physically analogous to the case where a particle impacts into water behind a plate through a prepunched hole. Since all but one of the test firings in References 8 and 9 were for un-punched plates, it took a higher kinetic energy than the threshold kinetic energy to fail the plate; some of the kinetic energy was absorbed by the plate, hence only a percentage of the impacting energy was transmitted to the water behind the plate.

The actual mechanism of the perforation of a plate after being impacted by a high speed projectile is quite complex. Immediately after impact strong shock waves are produced both in the plate and in the projectile. These shock waves, which initially are plane waves, are attenuated from the lateral free surfaces of the projectile; upon reaching the back surface of the projectile and the back surface of the plate they also reflect into rarefaction waves. Depending on the impact velocity and plate material, the viscoplastic effect may be important.

In general terms, there are three processes for energy dissipation during perforation. The first one is shock dissipation; it is well known that a shock wave is an irreversible process, across which kinetic energy is dissipated into heat energy. The second process of energy dissipation is the back splash of the projectile material. Strictly speaking, this is not a dissipation, but rather a transfer of part of the energy into the material that moves backward, not into the tank. The third process is the viscous dissipation; kinetic energy transfers into heat energy through viscosity of the material. For simplicity, it will be assumed that the viscous dissipation is negligible. For impact situations where the plate thickness is small compared with the projectile diameter it will be assumed that the other two processes combined will constitute a kinetic energy loss equal to the kinetic energy possessed by a cylinder of the plate material having a thickness twice that of a plate, a diameter equal to that of the projectile and traveling at a velocity equal to the original projectile velocity. Based on this assumption the perforation kinetic energy is calculated.

Shown in Table I is the results of calculated perforation energy and threshold energy for a few impact cases. The corresponding experimental results as reported in References 8 and 9 are also included in Table I.

It can be seen that the sum of the perforation energy and the threshold energy, which will be called the fracture kinetic energy, is in general agreement with the energy possessed by projectiles that actually perforated and burst fuel tanks during experiments.

TABLE I

CRITICAL KINETIC ENERGIES FOR 1/32" 7075 T-6 ALUMINUM PLATE

TEST	PRO- JECTILE DIAMETER (in)	PRO- JECTILE MATERIAL	PRE- PUNCHED PLATE	CALCULATED			EXPERIMENTAL
				THRESHOLD ENERGY (ft-lb) $(KE)_T$	PERFORATION ENERGY (ft-lb) $(KE)_P$	FRACTURE ENERGY (ft-lb) $(KE)_F = (KE)_T$ + $(KE)_P$	ENERGY THAT PRODUCED FRACTURE (ft-lb)
1.	7/32	Aluminum	yes	143	0	143	210 (Ref. 8)
2.	7/32	Aluminum	no	143	142	285	330 (Ref. 8)
3.	1/8	Aluminum	no	95	190	285	253 (Ref. 9)
4.	1/16	Steel	no	55	76	131	140 (Ref. 9)

VI CONCLUDING REMARKS

The problem being studied in this report is primarily for an unprotected fuel tank impacted by hypervelocity particles. If the velocity of the projectile is extremely high, it is conceivable that for a bumper-protected fuel tank the debris of the bumper and the projectile will still possess enough kinetic energy to penetrate the tank wall and create a high pressure region in the liquid fuel. For those cases the calculations performed in this report are still applicable. However, for a properly designed bumper-protected tank, the debris and the remnants of the projectile should not possess too much kinetic energy, and should not be able to puncture the main wall and create a high pressure region in the liquid fuel. In this case, the main wall is loaded primarily on the front face by the debris cloud of the impacted bumper. The pressure created in the liquid fuel will not be too high; the deflection of the wall will be inward, instead of the outward deflection of the unprotected wall. The problem of the stress, deflection, and failure of a bumper-protected wall will be studied in the next phase of this project.

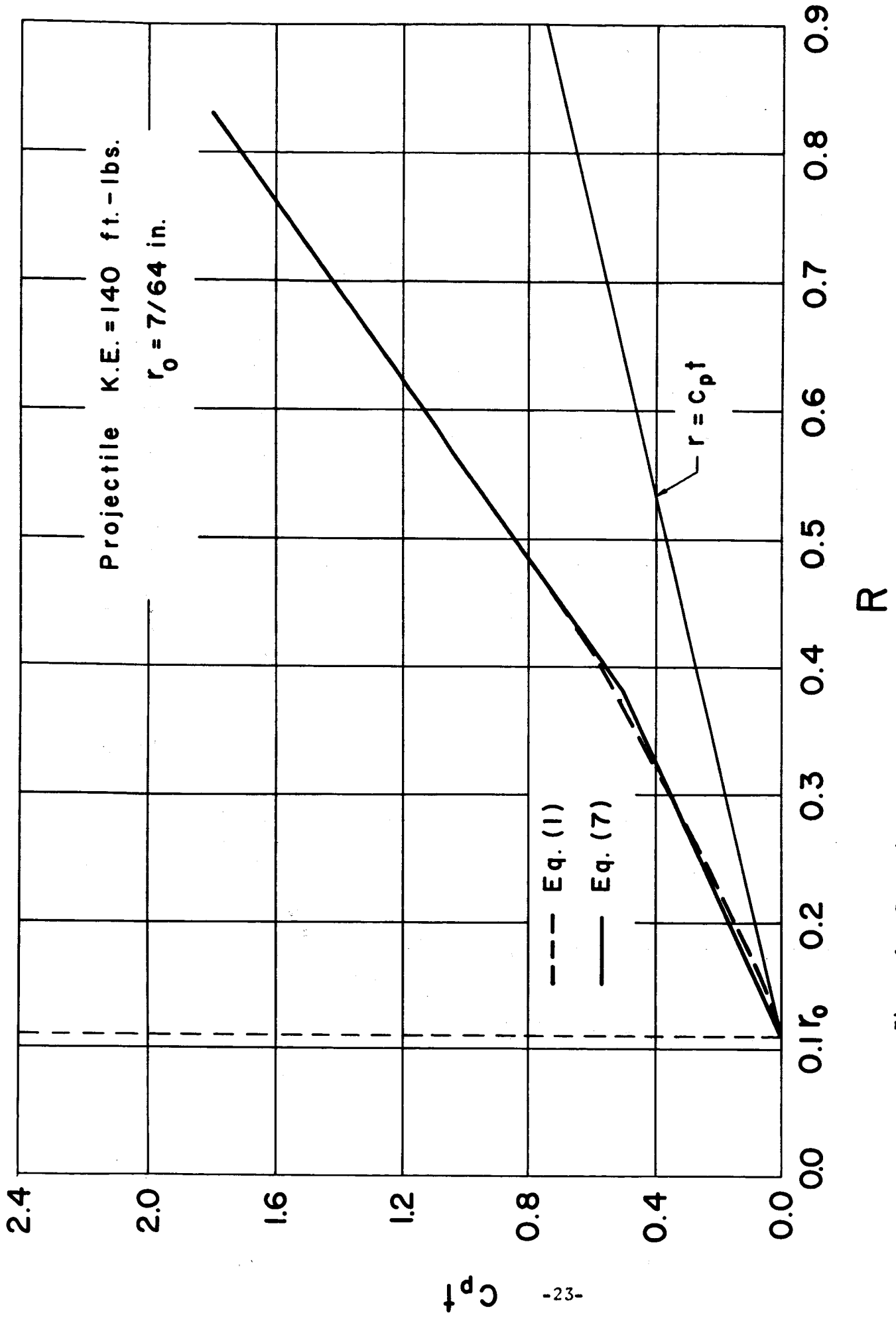


Figure 1. Comparison of the exact and approximate shock front positions, shock radius versus time, K.E. = 140 ft.-lbs, $r_0 = 7/64$ in.

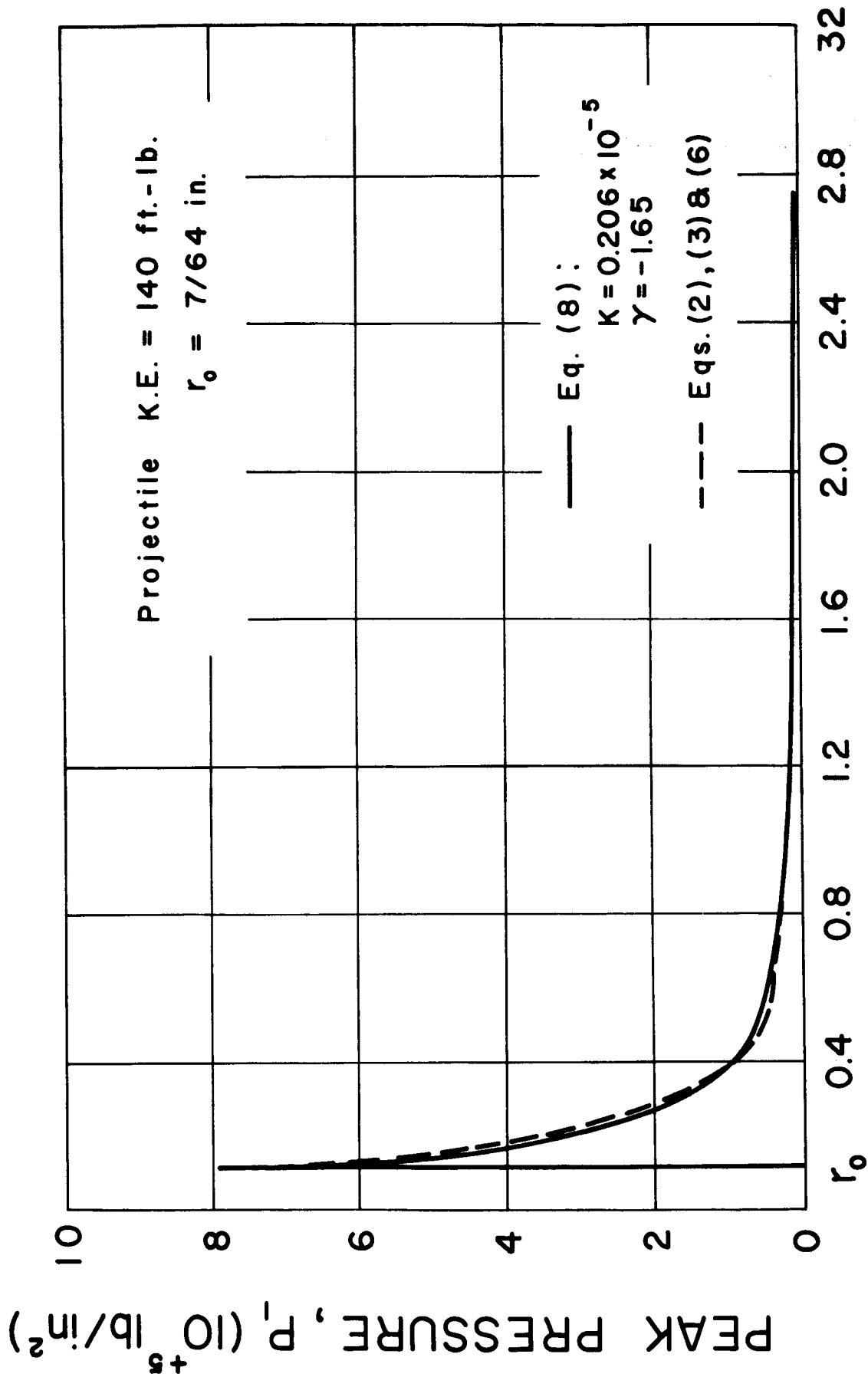


PLATE RADIUS, R (in.)

Figure 2. Comparison of the exact and approximate peak pressures as functions of radius, K.E. = 140 ft.-lbs, $r_0 = 7/64$ in.

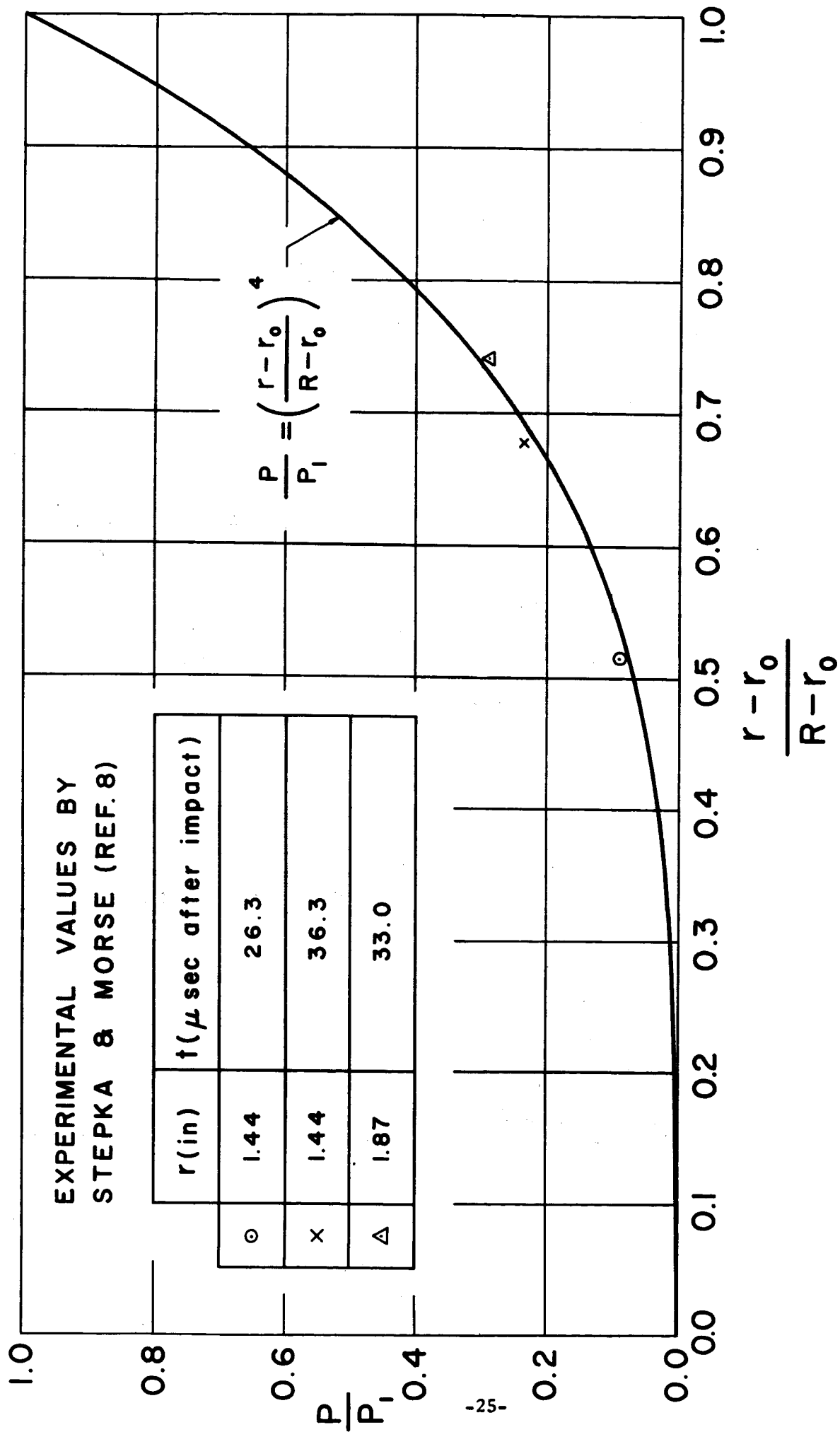


Figure 3. Pressure distribution behind the shock front in water due to impact.

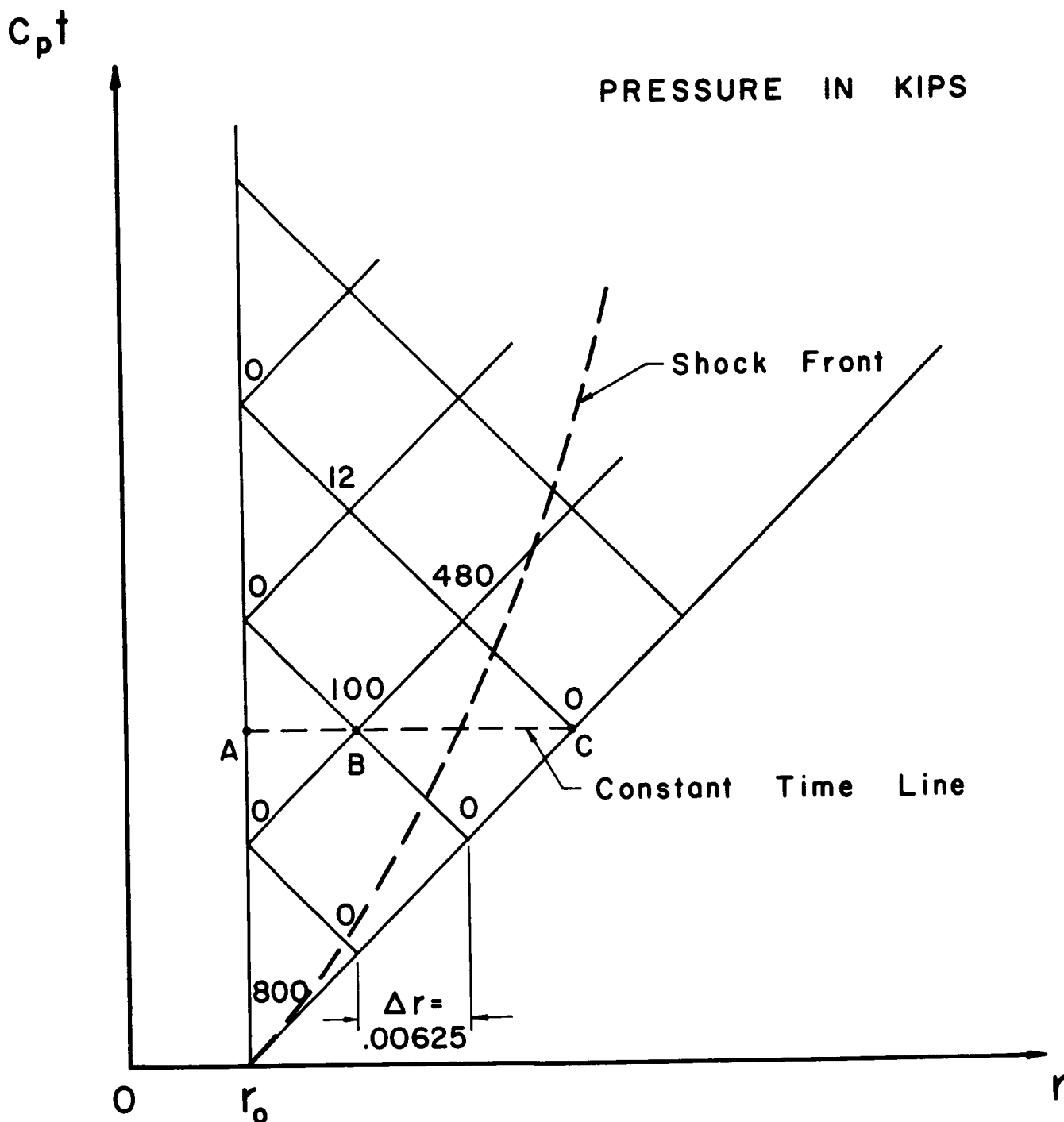


Figure 4. Values of the pressure at grid points during early time after impact.

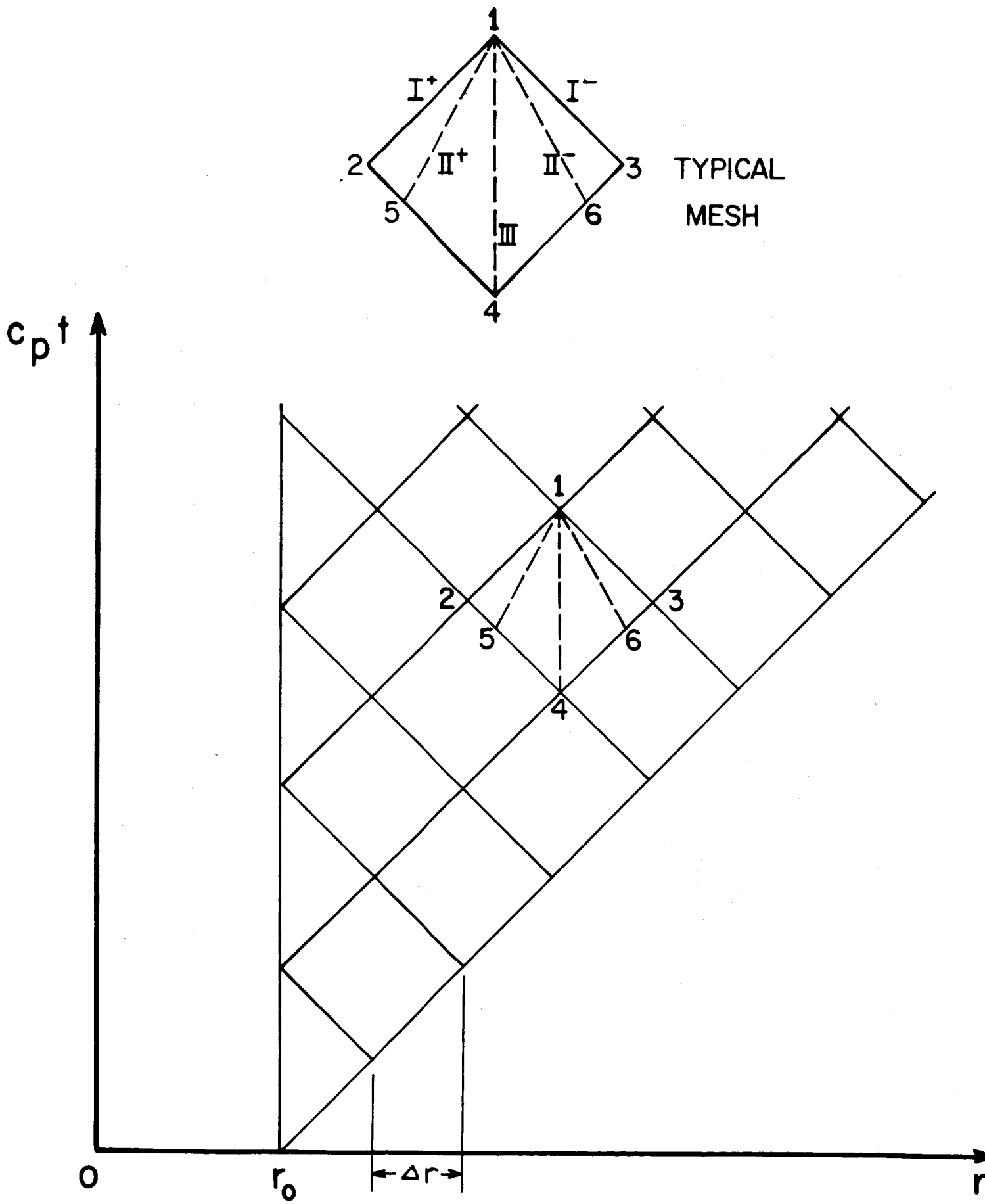


Figure 5. Characteristic Network for Application of Numerical Procedure .

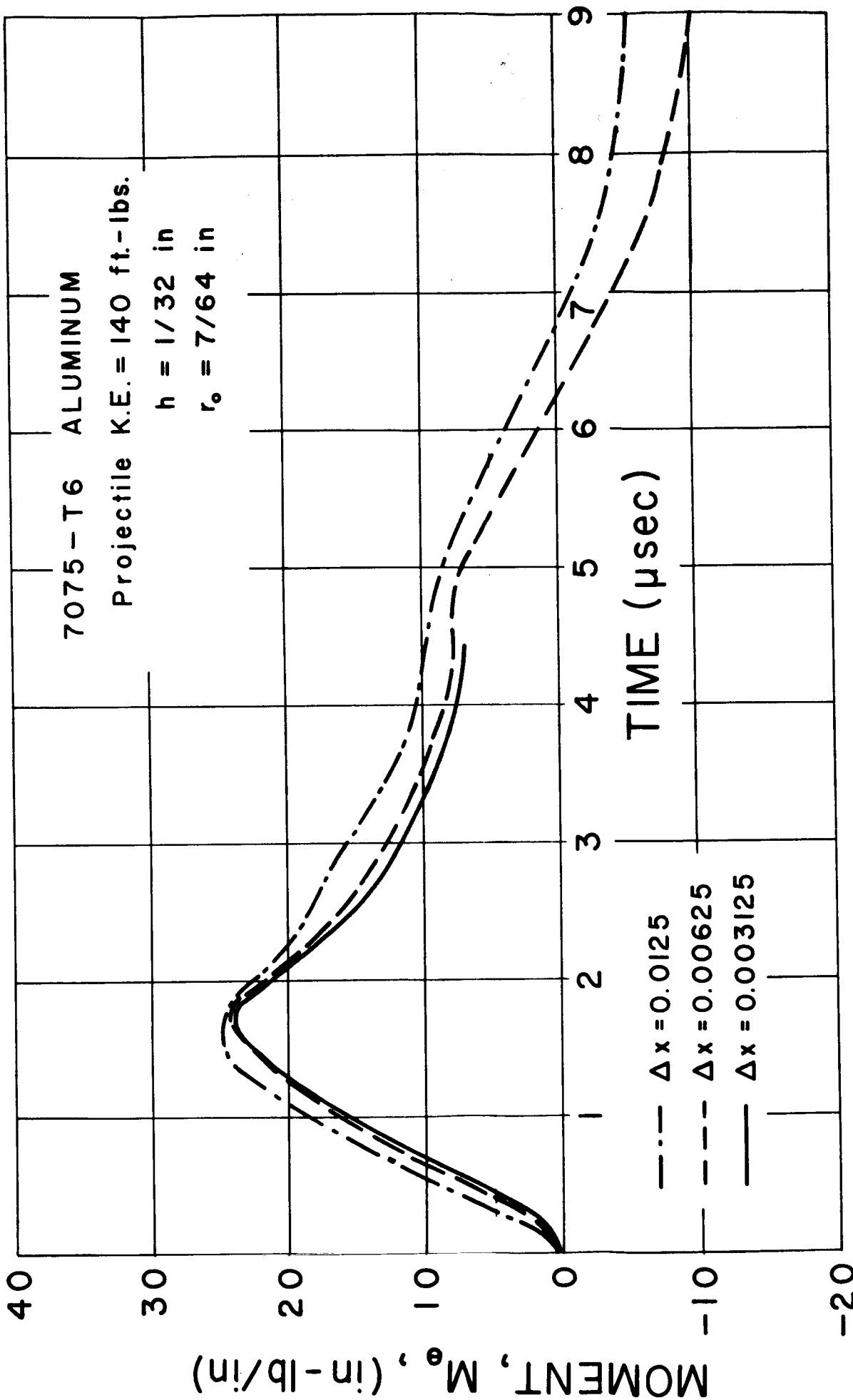
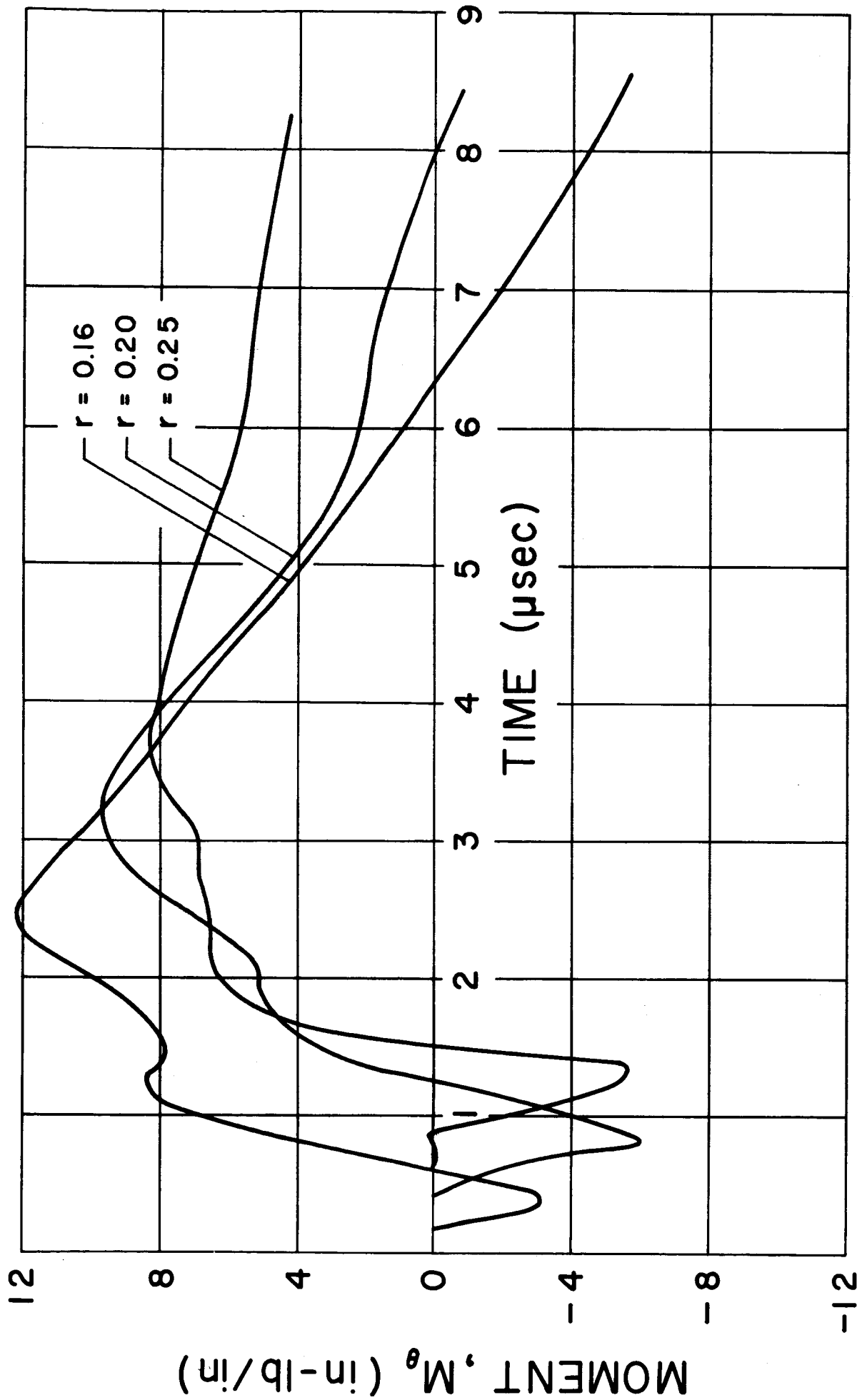
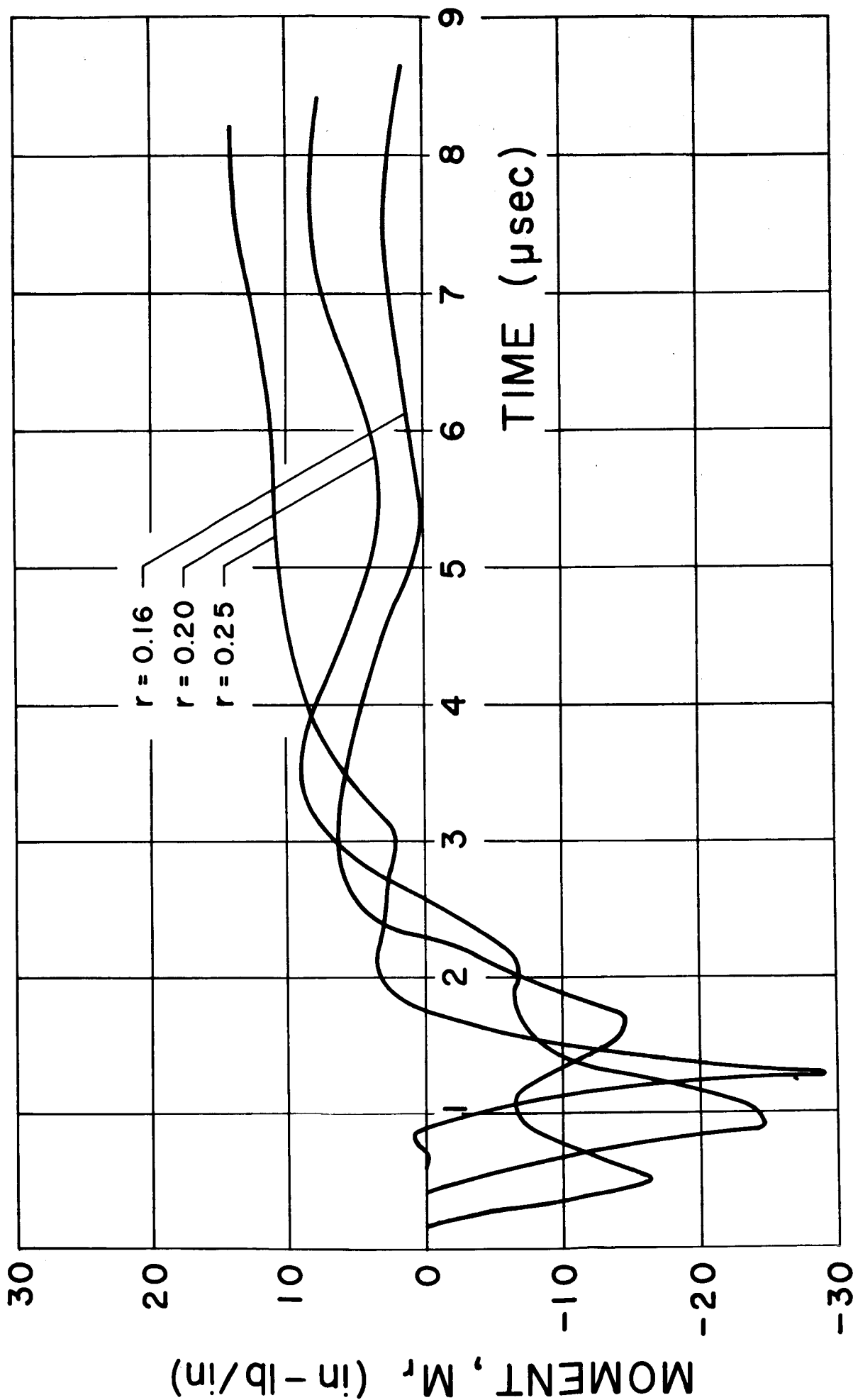


Figure 6. Comparison of the response of a plate, M_θ versus time at $r = r_0$, for three different mesh sizes, under a projectile kinetic energy input of 140 ft-lb, $r_0 = 7/64$ in., $h = 1/32$ in.

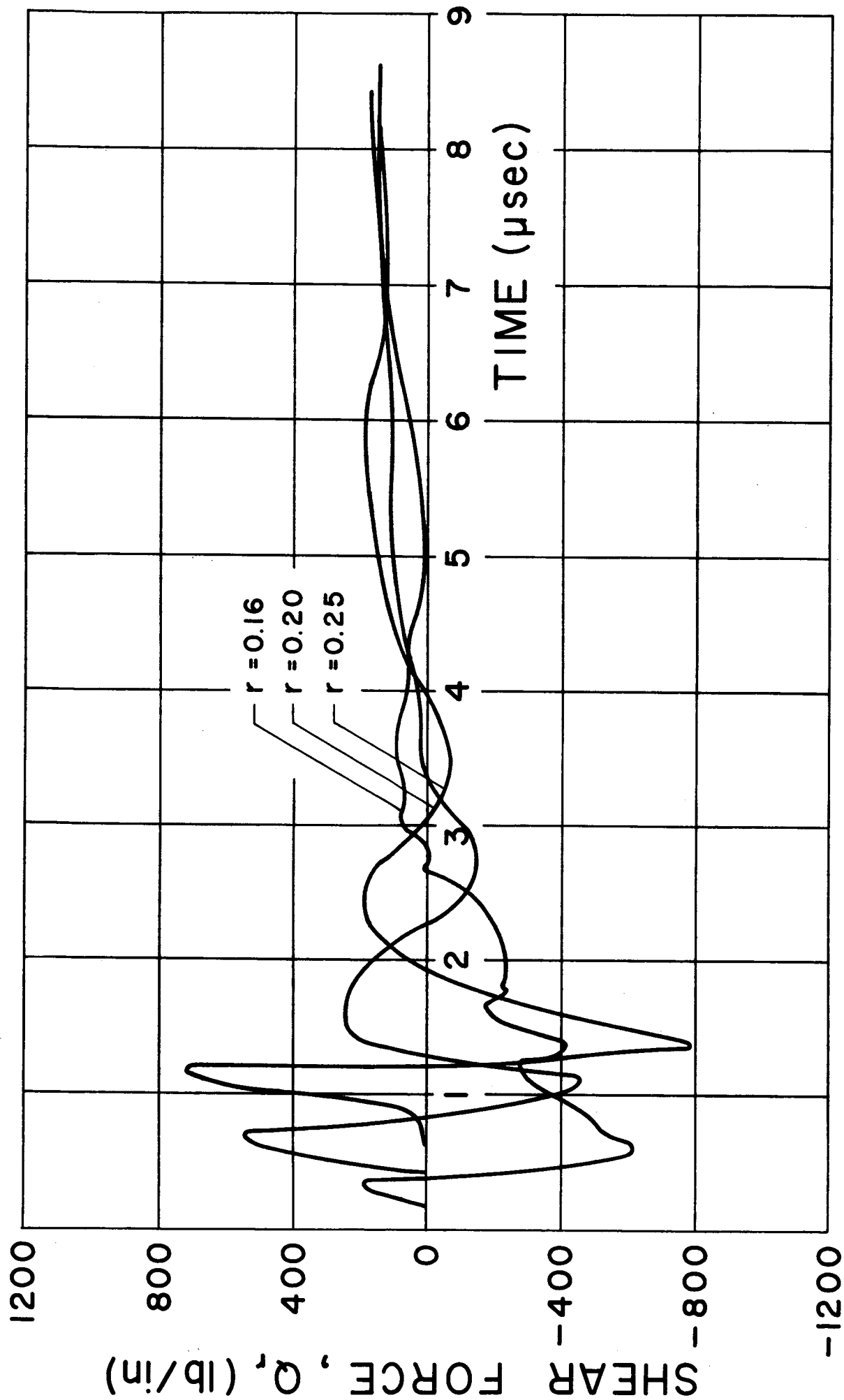


a. Moment M_θ versus time
 Figure 7. Response of a 7075-T6 aluminum plate at several radii under an impact kinetic energy of 140 ft-lb, $r_o = 7/64$ in., $h = 1/32$ in.



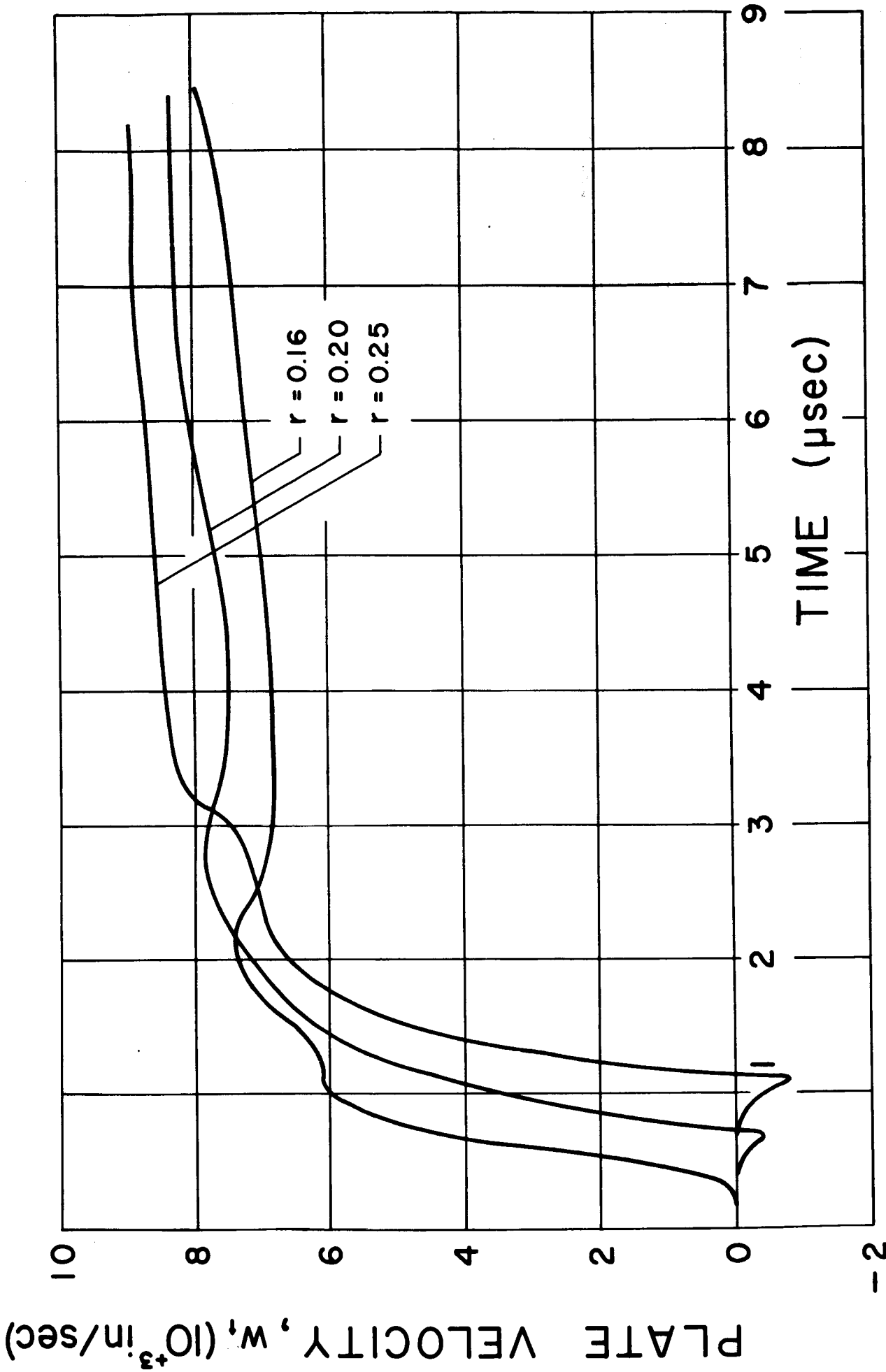
b. Moment M_r versus time

Figure 7. Response of a 7075-T6 aluminum plate at several radii under an impact kinetic energy of 140 ft-lb, $r_0 = 7/64$ in., $h = 1/32$ in.



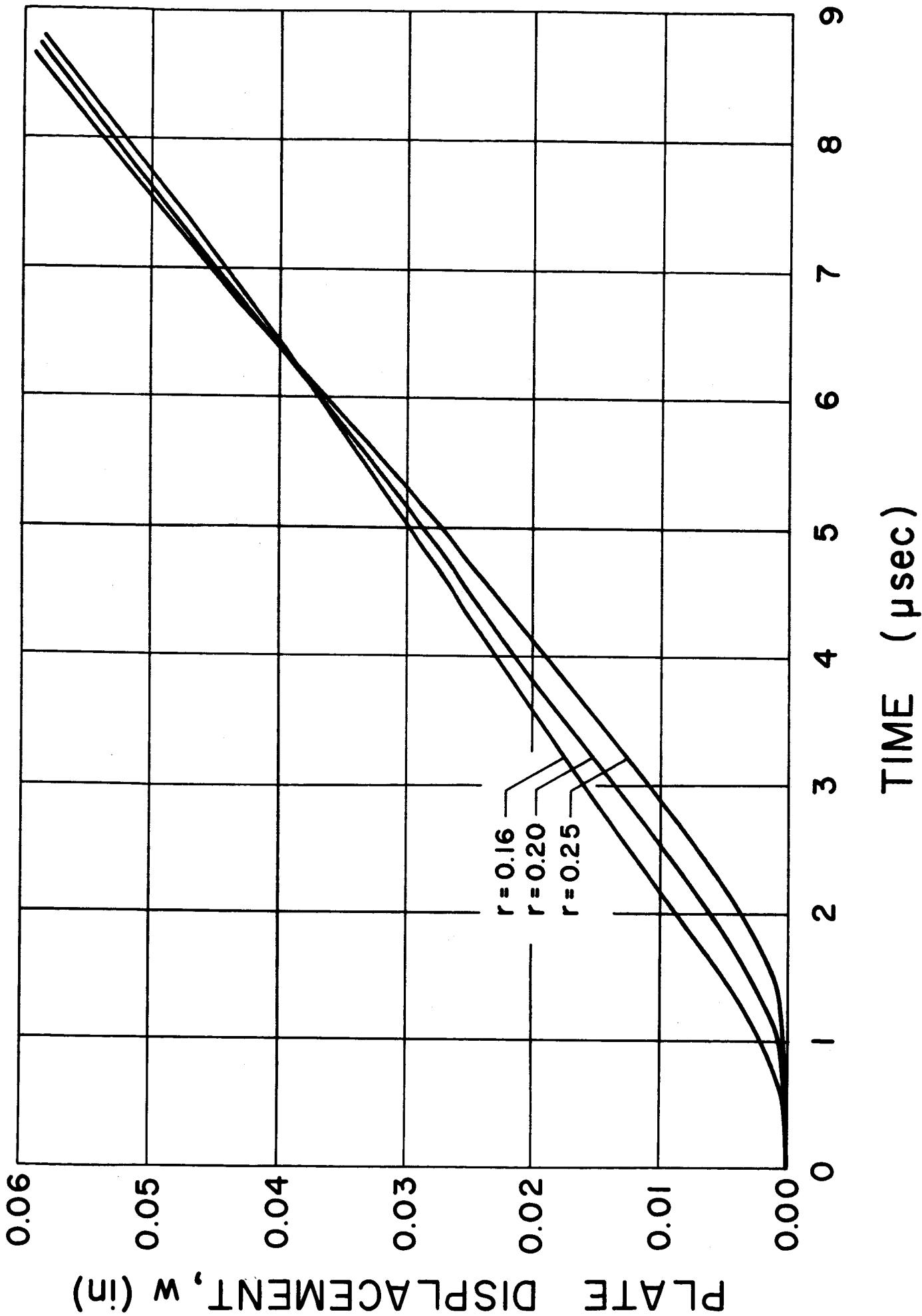
c. Shear force Q_r versus time

Figure 7. Response of a 7075-T6 aluminum plate at several radii under an impact kinetic energy of 140 ft-lb, $r_0 = 7/64$ in., $h = 1/32$ in.



d. Transverse velocity of the plate w_t versus time

Figure 7. Response of a 7075-T6 aluminum plate at several radii under an impact kinetic energy of 140 ft-lb, $r_0 = 7/64$ in., $h = 1/32$ in.



e. Transverse displacement of the plate w versus time

Figure 7. Response of a 7075-T6 aluminum plate at several radii under an impact kinetic energy of 140 ft-lb, $r_0 = 7/64$ in., $h = 1/32$ in.

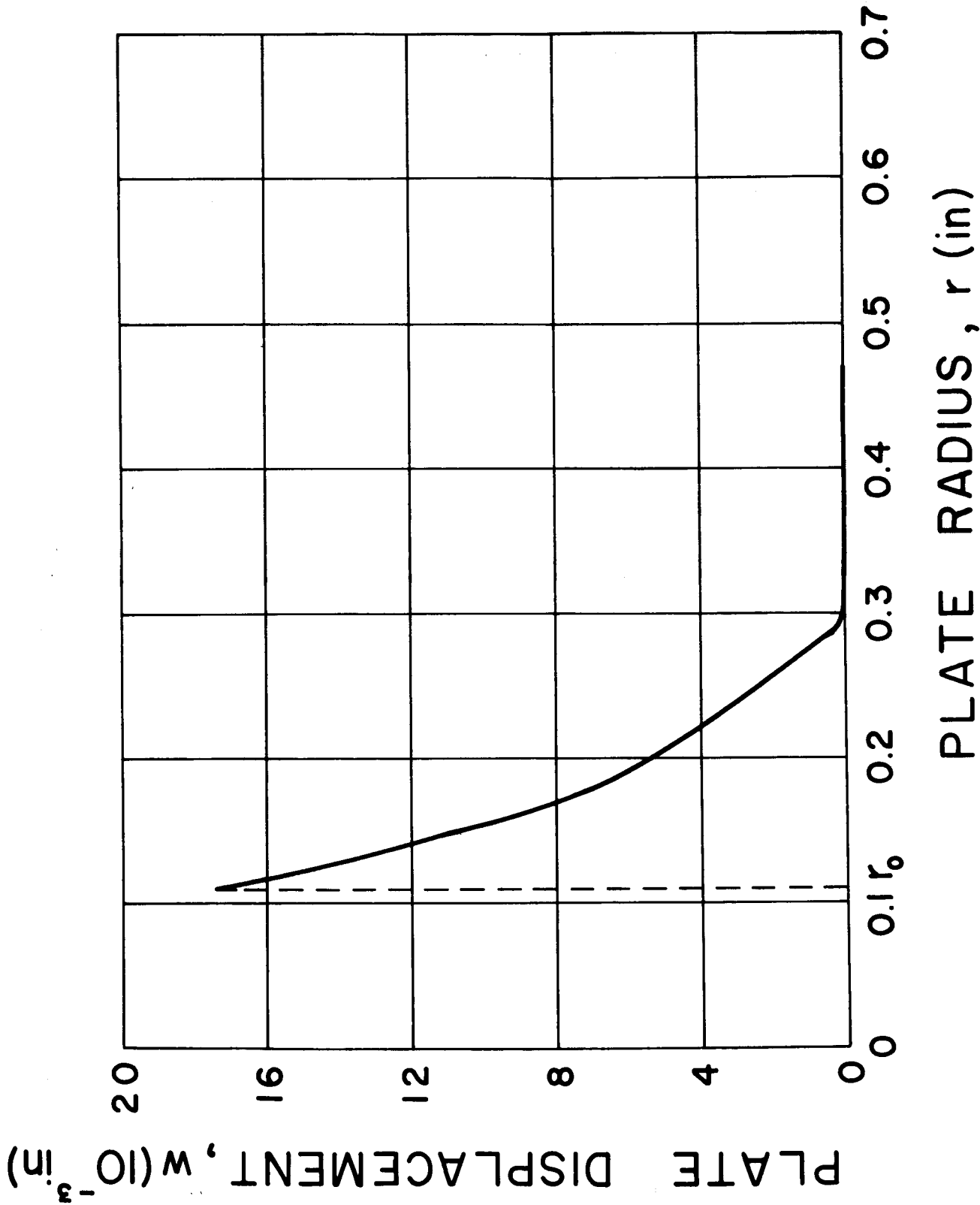


Figure 8. Transverse plate displacement versus radius, for a 1/64 in. thick 7075-T6 aluminum plate under a projectile kinetic energy of 50 ft-lb.

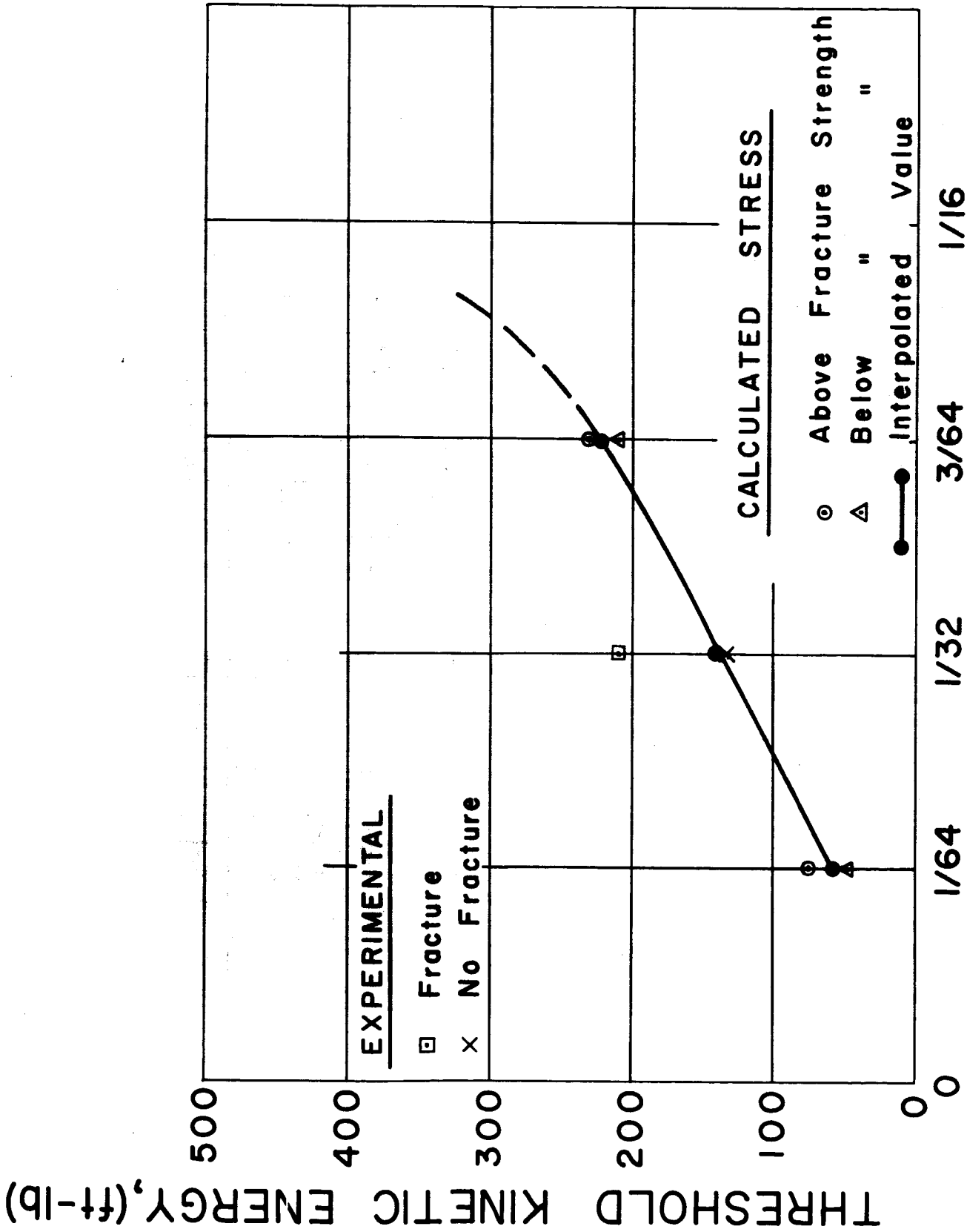


PLATE THICKNESS, h (in.)

Figure 9. Threshold kinetic energy versus plate thickness for 7075-T6 aluminum with an inner radius $r_0 = 7/64$ in.

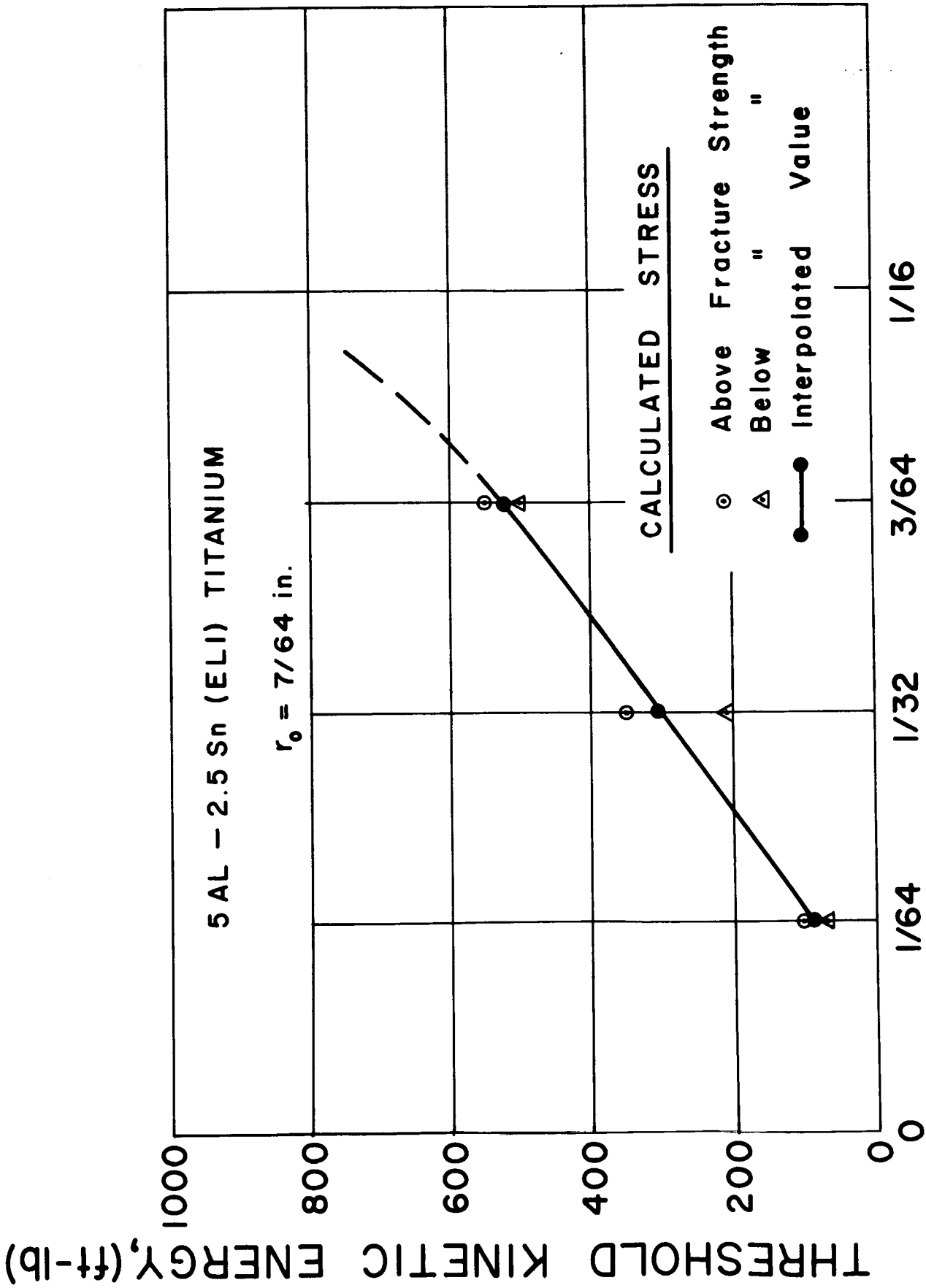


Figure 10. Threshold kinetic energy versus plate thickness for 5AL-2.5 Sn (ELI) titanium with an inner radius $r_0 = 7/64$ in.

TRESHOLD KINETIC ENERGY, (ft-lb)

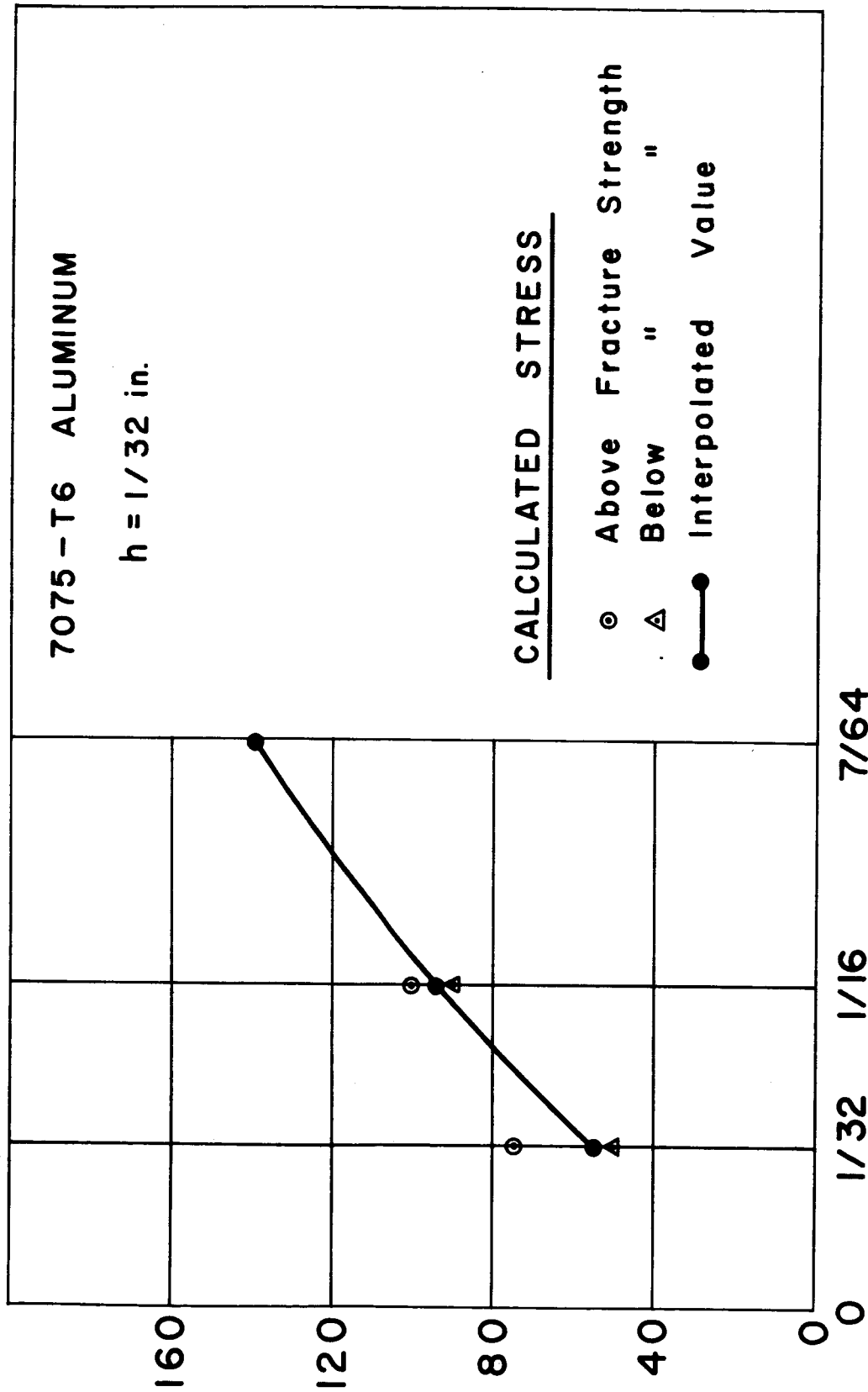


PLATE INNER RADIUS, r_0 (in.)

Figure 11. Threshold kinetic energy versus inner radius for 7075-T6 aluminum with a constant plate thickness, $h = 1/32$ in.

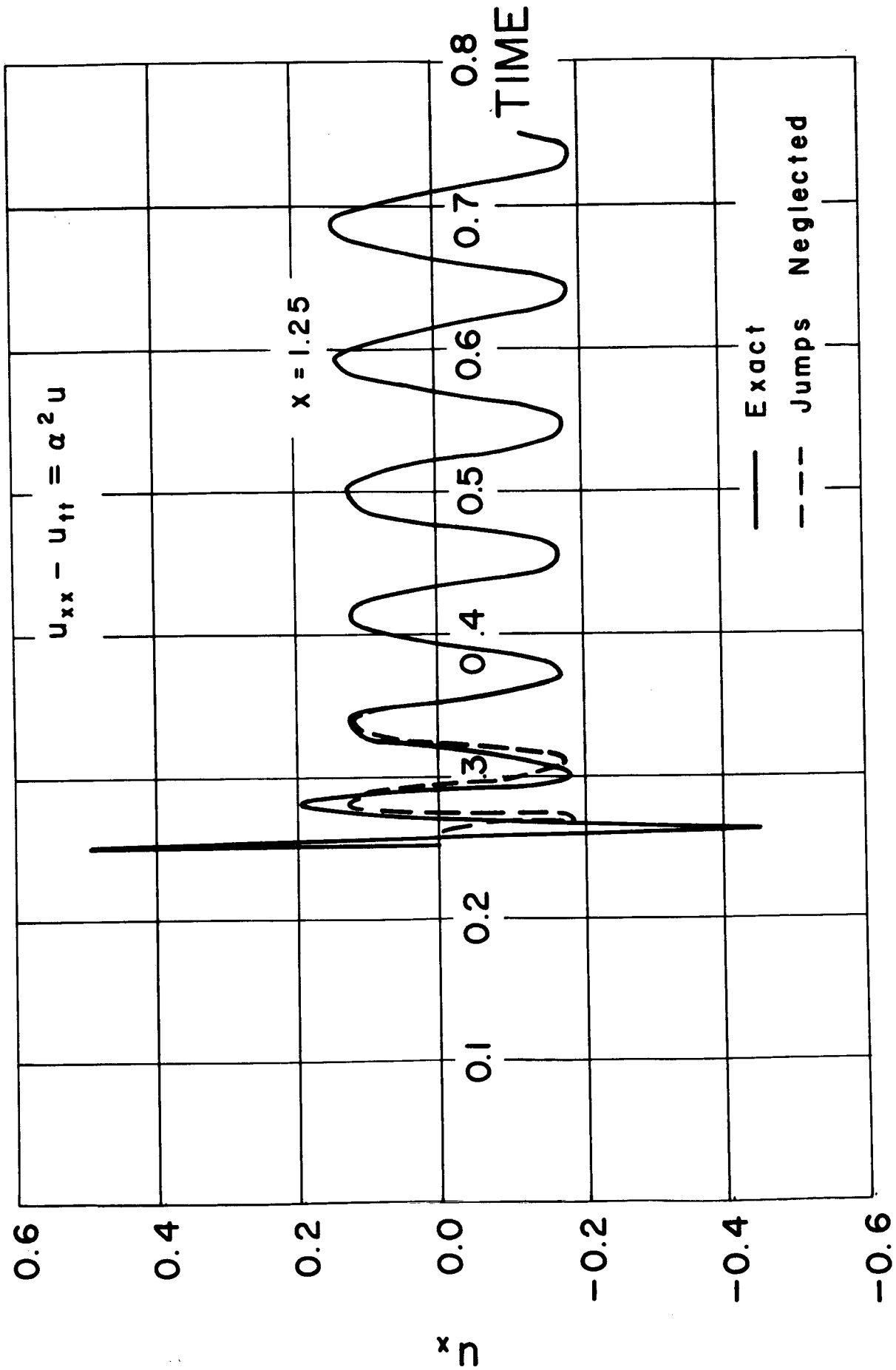


Figure 12. Comparison of "exact" numerical solution and approximate solution neglecting jump conditions.

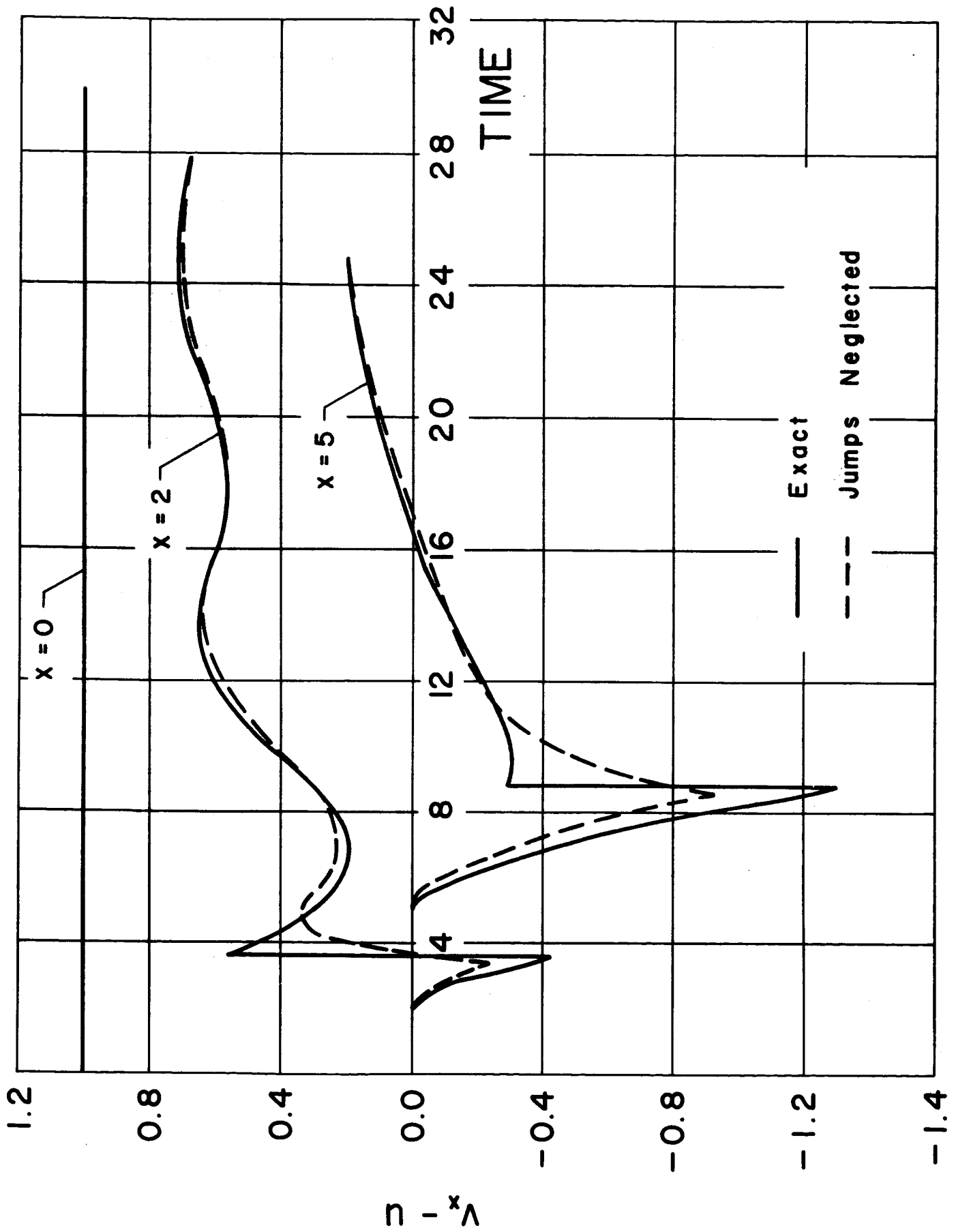


Figure 13. Comparison of "exact" numerical solution and approximate solution neglecting jump conditions for a Timoshenko beam.

VIII REFERENCES

1. Bull, C. V., et al., "Review of Hypervelocity Impact Studies at McGill University," Report No. 63-15, Dec. 1963.
2. Chou, P. C., "Perforation of Plates by High-Speed Projectiles," Vol. I of Developments in Mechanics, J. E. Lay and L. E. Malvern, eds., Plenum Press, 1961.
3. Chou, P. C., "Visco-Plastic Flow Theory in Hypervelocity Perforation of Plates," Proc. of the Fifth Symposium on Hypervelocity Impact, Vol. I, Pt. 1, Apr. 1962, pp. 307-328.
4. Kraus, H., "Two-Dimensional Analysis of a Hypervelocity Impact Upon a Visco-Plastic Plate," Proc. of the Sixth Symposium on Hypervelocity Impact, Vol. III, Aug. 1963, pp. 13-40.
(Sponsored by U. S. Army, U. S. Air Force and U. S. Navy.)
5. Kruszewski, E. J., "Protection of Spacecraft from Meteoroid Impact," presented at Highwater Laboratory Conference on Meteoroid Impact, July 14, 1966.
6. Watson, R. W., "The Perforation of Thin Plates by High Velocity Fragments," Proc. of the Fifth Symposium on Hypervelocity Impact," Vol. I, Pt. 2, Apr. 1962.
7. Maiden, C. J., and McMillan, A. R., "An Investigation of the Protection Afforded a Spacecraft by a Thin Shield," AIAA Journal, Vol. 2, No. 11, November 1964, pp. 1992-1998.
8. Stepka, F. S. and Morse, C. R., "Preliminary Investigation of Catastrophic Fracture of Liquid-filled Tanks Impacted by High-Velocity Particles," NASA TN D-1537, May 1963.

9. Morse, C. R. and Stepka, F. S., "Effect of Projectile Size and Material on Impact Fracture of Walls of Liquid-filled Tanks," NASA TN D-3627, September 1966.
10. Stepka, F.S., Morse, C. R. and Dengler, R. P., "Investigation of Characteristics of Pressure Waves Generated in Water-filled Tanks Impacted by High Velocity Projectiles," NASA TN D-3143, December 1965.
11. Ferguson, C. W., "Hypervelocity Impact Effects on Liquid Hydrogen Tanks," NASA CR-54852, March 31, 1966.
12. Chou, P. C., Sidhu, H. S. and Karpp, R. R., "Analysis of Peak Pressure Generated in Water by High Velocity Impact," DIT Report No. 160-1, NASA CR-50249, April 1963.
13. Chou, P. C. and Koenig, H. A., "Flexural Waves in Elastic Circular Plates by Method of Characteristics," DIT Report No. 160-6, August 1965.
14. Rice, M. H. and Walsh, J. H., "Equation of State of Water to 250 Kilobars," Journal of Chemical Physics, Vol. 26, P. 824, 1957.
15. Jahsman, W. E., "Propagation of Abrupt Circular Wave Fronts in Elastic Sheets and Plates," Proc. of the 3rd National Congress of Applied Mech., 1958, pp. 115-202.
16. Timoshenko S. and Woinowsky-Krieger, S., "Theory of Plates and Shells," McGraw-Hill Book Co. Inc., 2nd Edition, 1959, p. 108.
17. Timoshenko, S. and Woinowsky-Krieger, S., "Theory of Plates and Shells," McGraw-Hill Book Co. Inc., 2nd Edition, 1959, p. 82.
18. Rinehart, J. S., Pearson, J., "Behavior of Metals Under Impulsive Loads," American Society for Metals, 1954, p. 128.

19. Llorens, R. E., Chou, P. C. and Gold, L., "Axisymmetric Large Deflections of Circular Plates with a Central Hole," DIT Report No. 160-2, April 1963.
20. Chou, P. C. and Mortimer, R. W., "A Unified Approach to One-Dimensional Elastic Waves by the Method of Characteristics," DIT Report No. 160-8, NASA CR-78493, September 1966.
21. Boley, B. A. and Chao, C. C., "Some Solutions of the Timoshenko Beam Equations," Jour. of Appl. Mech., Vol. 77, 1955, pp. 579-586.

APPENDIX A

APPROXIMATE TREATMENT OF THE JUMP CONDITIONS

When a discontinuity in stresses, or in the derivatives of displacements, exists on the boundary, $r = r_0$, or on the initial value line, $t = 0$, it propagates along the characteristics in a manner as discussed in Ref. 20. In carrying out the numerical integrations of a problem, the location of these discontinuities in the r,t -plane must be traced and the jumps in all quantities must be accounted for. In the present problem where the applied load has a moving wave front, discontinuities are excited at every point on the wave front in the r,t -plane. If the propagation of these discontinuities were to be handled exactly, the numerical work would be prohibitive. In this appendix, it will be demonstrated by simple examples that the propagation of these discontinuities may be treated in a simple approximate manner. More specifically, the propagation of these discontinuities may be ignored completely.

In the first example, we shall consider the following differential equation governing the variable u ,

$$\frac{\partial^2 u}{\partial x^2} - \frac{\partial^2 u}{\partial t^2} = \alpha^2 u \quad (\text{A.1})$$

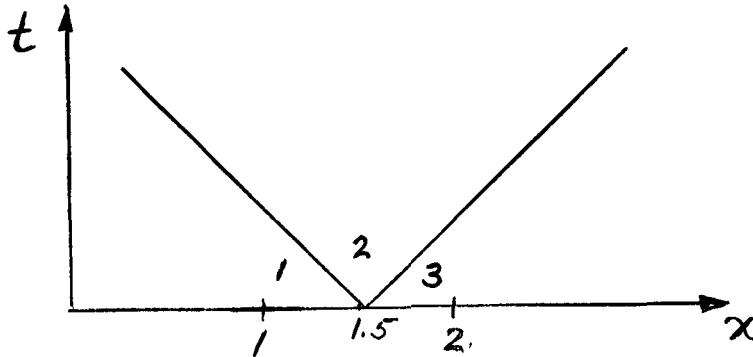
where a value of $\alpha^2 = 3664$ is used. An initial value problem is considered with the initial conditions at $t = 0$ as follows

$$\begin{aligned} u_t &= 0 && \text{for } -\infty < x < \infty \\ u &= 0 && \text{for } -\infty < x < 1.5 \\ u &= x - 1.5 && \text{for } 1.5 < x < \infty \end{aligned} \quad (\text{A.2})$$

Thus, u_x is 0 for $x < 1.5$, and 1 for $x > 1.5$, with a unit discontinuity at $x = 1.5$. From eq. (17) of Ref. 20, and the corresponding equation for C_k^- , we have

$$\begin{aligned} u_{x2} - u_{x3} &= - (u_{t2} - u_{t3}) \\ u_{x2} - u_{x1} &= (u_{t2} - u_{t1}) \end{aligned} \tag{A.3}$$

where subscripts 1, 2, and 3 refer to regions adjacent to the discontinuity point as shown below



Since it is known that $u_{x1} = 0$, $u_{x3} = 1$, and $u_{t1} = u_{t3} = 0$, it can be shown readily that the imposed discontinuity propagates along the line $x-t = 1.5$ with magnitudes

$$\begin{aligned} [u_x] &= -0.5, \\ [u_t] &= +0.5 \end{aligned} \tag{A.4}$$

and along $x+t = 1.5$ with

$$\begin{aligned} [u_x] &= +0.5, \\ [u_t] &= +0.5 \end{aligned} \tag{A.5}$$

Using these jump conditions and the numerical integration procedure of Ref. 20, the exact distribution of u is determined. Next, an approximate scheme which neglects all jumps across the lines $x \pm t = 1.5$, but otherwise unchanged, is used and an approximate field of u is calculated. A

comparison of the exact u field with the approximate one is demonstrated in Figure 12, where the u_x at $x = 1.25$ from the two calculations are plotted. As can be seen, the solution with no jump conditions differs from the one with correct jump conditions only during the first few oscillations. After this, the solutions merge and show little difference for all later times. The results at other x locations, and for u and u_t , are of the same form as those shown for u_x at $x = 1.25$.

The second example is a calculation made for a Timoshenko beam, with the governing equations in dimensionless form, (see Ref. 20).

$$\begin{aligned} u_{xx} - \frac{1}{c_1^2} u_{tt} &= f_2 u + f_3 v_x \\ v_{xx} - \frac{1}{c_2^2} v_{tt} &= g, u_x \end{aligned} \tag{A.6}$$

where subscripts x and t designate partial differentiations.

Values of the coefficients used are

$$\begin{aligned} c_1 &= 1 \\ c_2 &= 0.5774 \\ f_2 &= 1/3 \\ f_3 &= 1/3 \\ g_1 &= 1 \end{aligned}$$

which agree with those used in Ref. 21. The problem consists of a semi-infinite beam initially at rest and loaded suddenly at $x = 0$ by a constant shear force. This loading condition may be expressed as

$$\begin{aligned} \text{at } t = 0, 0 \leq x < \infty, u = v = u_t = v_t &= 0 \\ \text{at } x = 0, t > 0, v_x - u = 1, u_x &= 0 \end{aligned} \tag{A.7}$$

Thus, at $x = 0, t = 0$, a jump of $[v_x] = -c_2, [v_t] = 1$ is excited, which will propagate along the line $x - c_2 t = 0$ with undiminished magnitude. Again,

two sets of calculations were made, one with the correct jump conditions, the other neglecting the jumps. The results are shown in Figure 13 as shear force, Q , against time at two x locations. It can be seen that the discrepancy between calculations with and without jumps is very slight; except at the beginning, the two cases are almost the same. Plots of curves of other quantities, such as velocity and moment, indicate the same comparison is true. Calculations for other type of inputs for the Timoshenko beam show that jumps can always be neglected.

In conclusion, it can be said that neglecting jumps in the method of characteristics causes a relatively small difference in the results obtained. In all of the results plotted, the greatest error occurred at the time the discontinuity arrived, and, at long times the error became negligible. This fact is very significant, since it allows the simple solution of problems too complicated for the method of characteristics merely because of the existence of jump conditions.

APPENDIX B

COMPUTER PROGRAM FOR NUMERICAL CALCULATIONS

The program used for this problem is a very general one, which can also be used for all of the problems stated in Ref. 20. For this reason many of the input quantities in this program are not relevant to the problem studied in this report, but because of the general nature of the program they must still be defined. Other input quantities are dependent upon the parameters of the plate and may be expressed as simple functions of them, as will be seen below.

The following variables from the plate problem must be known:

r_0 in inches, h in inches, Kinetic Energy in ft-lb.

Material characteristics: E in lb/in² G in lb/in²

ν (dimensionless) K_2 (dimensionless)

c_p and c_2 in in/sec.

The input for the program consists of 37 cards, containing the following quantities in the formats given at the right:

- | | | |
|-----|----------------------------|----------|
| 1. | MZERO, MEFN1, MEFN2, MEFN3 | (14,312) |
| 2. | XZERO, P1NC | (2E15.8) |
| 3. | CEE1, CEE2 | (2E15.8) |
| 4. | VA1, VA2, XCUT1 | (3E15.8) |
| 5. | VB1, VB2, XCUT2 | (3E15.8) |
| 6. | VC1, VC2, XCUT3 | (3E15.8) |
| 7. | AKAY1, GAMA1 | (2E15.8) |
| 8. | AKAY2, GAMA2 | (2E15.8) |
| 9. | AKAY3, GAMA3 | (2E15.8) |
| 10. | A11, A21, A31, A41 | (4E15.8) |

11.	A51, A61, A71	(3E15.8)
12.	CONSA	(E15.8)
13.	B11, B21, B31, B41	(4E15.8)
14.	B51, B61, B71	(3E15.8)
15.	CONSB	(E15.8)
16.	C11, C21, C31, C41	(4E15.8)
17.	C51, C61, C71	(3E15.8)
18.	CONSC	(E15.8)
19.	CKF1, CKF2, CKF3, CKF4	(4E15.8)
20.	CKF5, CKF6	(2E15.8)
21.	CKG1, CKG2, CKG3, CKG4	(4E15.8)
22.	CKG5, CKG6	(2E15.8)
23.	CKH1, CKH2, CKH3, CKH4	(4E15.8)
24.	CKH5, CKH6	(2E15.8)
25.	CKF2A	(E15.8)
26.	AZ1, AZ2, AZ3, AZ4	(4E15.8)
27.	AZ5, AZ6, AZ7	(3E15.8)
28.	BZ1, BZ2, BZ3, BZ4	(4E15.8)
29.	BZ5, BZ6, BZ7	(3E15.8)
30.	CZ1, CZ2, CZ3, CZ4	(4E15.8)
31.	CZ5, CZ6, CZ7	(3E15.8)
32.	FUU1, FUJ2, FUUX1, FUUX2	(4E15.8)
33.	FUUT1, FUUT2	(2E15.8)
34.	FUV1, FUV2, FUVX1, FUVX2	(4E15.8)
35.	FUVT1, FUVT2	(2E15.8)
36.	FUW1, FUW2, FUWX1, FUWX2	(4E15.8)
37.	FUWT1, FUWT2	(2E15.8)

The following quantities remain invariant for the plate problem and are equal to the numbers indicated:

$$\text{MEFN1} = \text{MEFN2} = +3 \quad \text{MEFN3} = +2$$

$$\text{VA1} = \text{VA2} = \text{VB1} = \text{VB2} = 0.$$

$$\text{AKAY1} = \text{AKAY2} = \text{GAMA1} = \text{GAMA2} = 0.$$

$$\text{A31} = \text{A41} = \text{A51} = \text{A61} = \text{A71} = 0.$$

$$\text{CONSA} = 0.$$

$$\text{B11} = \text{B31} = \text{B41} = \text{B61} = \text{B71} = 0.$$

$$\text{CONSB} = 0.$$

$$\text{C11} = \text{C21} = \text{C31} = \text{C51} = \text{C61} = \text{C71} = 0. \quad \text{C41} = 1.$$

$$\text{CONSC} = 0.$$

$$\text{CKF1} = -1. \quad \text{CKF2} = 1.$$

$$\text{CKF3} = \text{CKF4} = \text{CKF6} = 0.$$

$$\text{CKG1} = \text{CKG2} = \text{CKG3} = \text{CKG4} = \text{CKG5} = \text{CKG6} = 0.$$

$$\text{CKH1} = \text{CKH2} = \text{CKH5} = -1.$$

$$\text{CKH3} = \text{CKH4} = \text{CKH6} = 0.$$

$$\text{AZ2} = \text{AZ3} = \text{AZ4} = \text{AZ5} = \text{AZ6} = 0.$$

$$\text{BZ1} = \text{BZ3} = \text{BZ4} = \text{BZ6} = \text{BZ7} = 0.$$

$$\text{CZ2} = \text{CZ3} = \text{CZ4} = \text{CZ5} = \text{CZ6} = 0.$$

$$\text{FUU1} = \text{FUU2} = \text{FUUX1} = \text{FUUX2} = \text{FUUT1} = \text{FUUT2} = 0.$$

$$\text{FUV1} = \text{FUV2} = \text{FUVX1} = \text{FUVX2} = \text{FUVT1} = \text{FUVT2} = 0.$$

$$\text{FUW1} = \text{FUW2} = \text{FUWX1} = \text{FUWX2} = \text{FUWT1} = \text{FUWT2} = 0.$$

The following quantities vary with the variables of the plate problem as follows:

MZERO = number of points along $t = 0$ line (and thus also along boundary) at which properties are to be evaluated.

$$\text{XZERO} = r_0 \quad \text{PINC} = \Delta r \quad \text{XCUT1} = \text{XCUT2} = r_0$$

$$\text{CEE1} = c_p \quad \text{CEE2} = k_2 c_2$$

VC1 and VC2 = velocities from eq. (7) which approximates actual shock for a given kinetic energy.

XCUT3 = radius at which shock wave velocity changes from VC1 to VC2.

AKAY3 = $\frac{-K}{k_2^2 Gh}$ and GAMA = γ in the expression for peak pressure along the shock front: $P_o = Kr^Y$

$$A11 = D, \quad A21 = \frac{Dv}{r_o}$$

$$B21 = B51 = K_2^2 Gh$$

$$CKF5 = \frac{K_2^2 Gh}{D}$$

$$CKF2A = \frac{K_2^2 Gh}{D}$$

$$AZ1 = D, \quad AZ7 = Dv$$

$$BZ2 = BZ5 = K_2^2 Gh$$

$$CA1 = Dv, \quad CZ7 = D$$

The output of the program gives the values of several variables at all points in the physical plane. The quantities printed out, as they appear in the output, are:

$$\begin{array}{cccccccccc} r, & t, & 0, & 0, & \frac{P}{k_2^2 Gh}, & \phi, & \phi_x, & \phi_t, & & \\ 0, & 0, & 0, & w, & w_x, & w_t, & M_r, & Q_r, & M_\theta & \end{array}$$

The quantities which are listed as being printed out as zero at all points have no significance for this problem. Some small truncation error is introduced in the evaluation of the systems of equations at each point. The values of M_r and Q_r at the boundary are many orders of magnitude smaller than those at all interior points. Thus, they may effectively be considered to be zero. On the following pages is a listing of the general computer code that was used in the analysis of the examples presented in this report.

COMPUTER CODE
UNITS IN IN-LB-SEC SYSTEM

LIBFTC N=3ML

DIMENSIONX(2,300),T(2,300),PL1(2,300),PL2(2,300),PL3(2,300),U(2,300),UX(2,300),UT(2,300),V(2,300),VX(2,300),VT(2,300),W(2,300),WX(2,300),WT(2,300),Y(6,6),Z(6),UU(6)

C INPUT FORMATS

1 FORMAT(I4,3I2)
2 FORMAT(2E15.3)
3 FORMAT(3E15.8)
7 FORMAT(E15.8)

120 FORMAT(4E15.8)

C OUTPUT FORMATS

4 FORMAT(1H ,35HNUMBER OF POINTS ALONG T=0. LINE = ,I4)
5 FORMAT(1H ,8HXZERO = ,E15.8,5X,9HDELTA X = ,E15.8)
6 FORMAT(1H ,5H C1 = ,E15.8,5X,5H C2 = ,E15.8)
8 FORMAT(1H ,/)
9 FORMAT(1H ,6HVA1 = ,E15.8,5X,6HVA2 = ,E15.8,5X,8HXCUT1 = ,E15.8)
10 FORMAT(1H ,40HLOAD 1 UNIFORM TO LEFT OF LINE FOR ANY T)
11 FORMAT(1H ,52HLOAD 1 LINEARLY DECREASING TO LEFT OF LINE FOR ANY T
1)
12 FORMAT(1H ,30HLOAD 1 CONCENTRATED ALONG LINE)
13 FORMAT(1H ,21HLOAD 1 ALONG LINE = (,E15.8,6H)/X**,(,E15.8,1H))
804 FORMAT(1H ,6HVB1 = ,E15.8,5X,6HVB2 = ,E15.8,5X,8HXCUT2 = ,E15.8)
805 FORMAT(1H ,6HVC1 = ,E15.8,5X,6HVC2 = ,E15.8,5X,8HXCUT3 = ,E15.8)
806 FORMAT(1H ,40HLOAD 2 UNIFORM TO LEFT OF LINE FOR ANY T)
807 FORMAT(1H ,52HLOAD 2 LINEARLY DECREASING TO LEFT OF LINE FOR ANY T
1)
808 FORMAT(1H ,30HLOAD 2 CONCENTRATED ALONG LINE)
809 FORMAT(1H ,21HLOAD 2 ALONG LINE = (,E15.8,6H)/X**,(,E15.8,1H))
810 FORMAT(1H ,40HLOAD 3 UNIFORM TO LEFT OF LINE FOR ANY T)
811 FORMAT(1H ,52HLOAD 3 LINEARLY DECREASING TO LEFT OF LINE FOR ANY T
1)
812 FORMAT(1H ,30HLOAD 3 CONCENTRATED ALONG LINE)
813 FORMAT(1H ,21HLOAD 3 ALONG LINE = (,E15.8,6H)/X**,(,E15.8,1H))
14 FORMAT(1H ,7X,1HX,15X,1HT,13X,6HLOAD 1,10X,6HLOAD 2,10X,6HLOAD 3,1
12X,1HU,15X,2HUX,14X,2HUT)
122 FORMAT(1H ,7X,1HV,14X,2HVX,14X,2HVT,15X,1HW,14X,2HWX,14X,2HWT,12X,
12HS1,11X,2HS2,11X,2HS3,//)
800 FORMAT(1H ,8(E15.8,1X),1HO)
801 FORMAT(1H ,8(E15.8,1X),1HB)
802 FORMAT(1H ,8(E15.8,1X),1HI)
803 FORMAT(1H ,8(E15.8,1X),1HT)
121 FORMAT(1H ,6(E15.8,1X),2(E11.4,1X),E11.4)
17 FORMAT(1H ,36HMAIN DIAGONAL OF SOLUTION MATRIX FOR)
5960 FORMAT(1H ,33HTHIS POINT CONTAINS A 0. ELEMENT.)
124 FORMAT(1H ,6HS1 = (,E15.8,6H)*UX+(,E15.8,5H)*U+(,E15.8,6H)*VX+(,E1
15.8,5H)*V+(,E15.8,6H)*WX+(,E15.8,4H)*W+)
125 FORMAT(1H ,2H+(,E15.3,5H)*U/X)
126 FORMAT(1H ,6HS2 = (,E15.8,6H)*UX+(,E15.8,5H)*U+(,E15.8,6H)*VX+(,E1
15.8,5H)*V+(,E15.8,6H)*WX+(,E15.8,4H)*W+)
9817 FORMAT(1H ,6HS3 = (,E15.8,6H)*UX+(,E15.8,5H)*U+(,E15.3,6H)*VX+(,E1
15.8,5H)*V+(,E15.8,6H)*WX+(,E15.8,4H)*W+)
127 FORMAT(1H ,4HA1= ,E15.8)
128 FORMAT(1H ,4HB1= ,E15.8)
129 FORMAT(1H ,4HC1= ,E15.8)
130 FORMAT(1H ,1H(,E15.8,6H)*UX+(,E15.8,5H)*U+(,E15.8,6H)*VX+(,E15.8,5

```

      1H)*V+(,E15.8,6H)*WX+(,E15.8,4H)*W+)
131 FORMAT(1H ,2H+(,E15.8,7H)*UT=A1)
132 FORMAT(1H ,2H+(,E15.8,7H)*VT=B1)
133 FORMAT(1H ,2H+(,E15.8,7H)*WT=C1)
134 FORMAT(1H ,7HFU01 = ,E15.8,3X,7HFU02 = ,E15.8,3X,8HFU0X1 = ,E15.8,
      13X,8HFU0X2 = ,E15.8)
7031 FORMAT(1H ,8HFU0T1 = ,E15.8,3X,8HFU0T2 = ,E15.8)
135 FORMAT(1H ,6HF1 = (,E15.8,3H)/X)
136 FORMAT(1H ,6HF2 = (,E15.8,8H)/X**2+(,E15.8,1H))
137 FORMAT(1H ,5HF3 = ,E15.8)
138 FORMAT(1H ,5HF4 = ,E15.8)
139 FORMAT(1H ,5HF5 = ,E15.8)
140 FORMAT(1H ,5HF6 = ,E15.8)
141 FORMAT(1H ,5HG1 = ,E15.8)
142 FORMAT(1H ,5HG2 = ,E15.8)
143 FORMAT(1H ,5HG3 = ,E15.8)
144 FORMAT(1H ,5HG4 = ,E15.8)
145 FORMAT(1H ,5HG5 = ,E15.8)
146 FORMAT(1H ,5HG6 = ,E15.8)
147 FORMAT(1H ,5HH1 = ,E15.8)
148 FORMAT(1H ,6HH2 = (,E15.8,3H)/X)
149 FORMAT(1H ,5HH3 = ,E15.8)
150 FORMAT(1H ,5HH4 = ,E15.8)
151 FORMAT(1H ,6HH5 = (,E15.8,3H)/X)
152 FORMAT(1H ,5HH6 = ,E15.8)
153 FORMAT(1H ,7HFUV1 = ,E15.8,3X,7HFUV2 = ,E15.8,3X,8HFUVX1 = ,E15.8,
      13X,8HFUVX2 = ,E15.8)
7032 FORMAT(1H ,8HFUVT1 = ,E15.8,3X,8HFUVT2 = ,E15.8)
154 FORMAT(1H ,7HFUW1 = ,E15.8,3X,7HFUW2 = ,E15.8,3X,8HFUWX1 = ,E15.8,
      13X,7HFUWX2 = ,E15.8)
7033 FORMAT(1H ,8HFUWT1 = ,E15.8,3X,8HFUWT2 = ,E15.8)
C
  READ INPUT DATA
  READ 1,MZERO,MEFN1,MEFN2,MEFN3
  READ 2,XZERO,PINC
  READ 2,CEE1,CEE2
  READ 3,VA1,VA2,XCUT1
  READ 3,VB1,VB2,XCUT2
  READ 3,VC1,VC2,XCUT3
  READ 2,AKAY1,GAMA1
  READ 2,AKAY2,GAMA2
  READ 2,AKAY3,GAMA3
  READ 120,A11,A21,A31,A41
  READ 3,A51,A61,A71
  READ 7,CUNSA
  READ 120,B11,B21,B31,B41
  READ 3,B51,B61,B71
  READ 7,CONSB
  READ 120,C11,C21,C31,C41
  READ 3,C51,C61,C71
  READ 7,CONSC
  READ 120,CKF1,CKF2,CKF3,CKF4
  READ 2,CKF5,CKF6
  READ 120,CKG1,CKG2,CKG3,CKG4
  READ 2,CKG5,CKG6
  READ 120,CKH1,CKH2,CKH3,CKH4

```

```

READ 120,CKG1,CKG2,CKG3,CKG4
READ 2,CKG5,CKG6
READ 120,CKH1,CKH2,CKH3,CKH4
READ 2,CKH5,CKH6
READ 7,CKF2A
READ 120,AZ1,AZ2,AZ3,AZ4
READ 3,AZ5,AZ6,AZ7
READ 120,BZ1,BZ2,BZ3,BZ4
READ 3,BZ5,BZ6,BZ7
READ 120,CZ1,CZ2,CZ3,CZ4
READ 3,CZ5,CZ6,CZ7
READ 120,FUU1,FUU2,FUUX1,FUUX2
READ 2,FUUT1,FUUT2
READ 120,FUV1,FUV2,FUVX1,FUVX2
READ 2,FUVT1,FUVT2
READ 120,FUW1,FUW2,FUWX1,FUWX2
READ 2,FUWT1,FUWT2
EM=CEE1/CEE2
FAK1=(EM-1.)/(2.*EM)
FAK2=(EM-1.)/(EM+1.)
C PRINT ELEGANT PRELIMINARY PRINTOUT
PRINT 8
PRINT 4,MZERO
PRINT 5,XZERO,PINC
PRINT 6,CEE1,CEE2
PRINT 9,VA1,VA2,XCUT1
PRINT 804,VB1,VB2,XCUT2
PRINT 805,VC1,VC2,XCUT3
PRINT 13,AKAY1,GAMA1
GO TO (15,16,123),MEFN1
15 PRINT 10
GO TO 18
16 PRINT 11
GO TO 18
123 PRINT 12
18 PRINT 809,AKAY2,GAMA2
GO TO (814,815,816),MEFN2
814 PRINT 806
GO TO 817
815 PRINT 807
GO TO 817
816 PRINT 808
817 PRINT 813,AKAY3,GAMA3
GO TO (818,819,820),MEFN3
818 PRINT 810
GO TO 821
819 PRINT 811
GO TO 821
820 PRINT 812
821 PRINT 130,A11,A21,A31,A41,A51,A61
PRINT 131,A71
PRINT 127,CONSA
PRINT 130,B11,B21,B31,B41,B51,B61
PRINT 132,B71
PRINT 128,CONSB

```

```
PRINT 130,C11,C21,C31,C41,C51,C61
PRINT 133,C71
PRINT 129,CONSC
PRINT 134,FUU1,FUU2,FUUX1,FUUX2
PRINT 7031,FUUT1,FUUT2
PRINT 153,FUV1,FUV2,FUVX1,FUVX2
PRINT 7032,FUVT1,FUVT2
PRINT 154,FUW1,FUW2,FUWX1,FUWX2
PRINT 7033,FUWT1,FUWT2
PRINT 135,CKF1
PRINT 136,CKF2,CKF2A
PRINT 137,CKF3
PRINT 138,CKF4
PRINT 139,CKF5
PRINT 140,CKF6
PRINT 141,CKG1
PRINT 142,CKG2
PRINT 143,CKG3
PRINT 144,CKG4
PRINT 145,CKG5
PRINT 146,CKG6
PRINT 147,CKH1
PRINT 148,CKH2
PRINT 149,CKH3
PRINT 150,CKH4
PRINT 151,CKH5
PRINT 152,CKH6
PRINT 124,AZ1,AZ2,AZ3,AZ4,AZ5,AZ6
PRINT 125,AZ7
PRINT 126,BZ1,BZ2,BZ3,BZ4,BZ5,BZ6
PRINT 125,BZ7
PRINT 9817,CZ1,CZ2,CZ3,CZ4,CZ5,CZ6
PRINT 125,CZ7
PRINT 8
PRINT 14
PRINT 122
GO TO 100
```

```
C LOAD DEFINITIONS
20 GO TO (850,851,852),IDIOT
850 V1=VA1
V2=VA2
XCUT=XCUT1
AKAY=AKAY1
GAMMA=GAMA1
NSTOP=NS1
MEFN=MEFN1
GO TO 860
851 V1=VB1
V2=VB2
XCUT=XCUT2
AKAY=AKAY2
GAMMA=GAMA2
NSTOP=NS2
MEFN=MEFN2
GO TO 860
```

```

852 V1=VC1
    V2=VC2
    XCUT=XCUT3
    AKAY=AKAY3
    GAMMA=GAMA3
    NSTOP=NS3
    MEFN=MEFN3
860 GO TO (21,41,61),MEFN
C   LOAD UNIFORM TO LEFT OF LINE FOR ANY T
    21 IF(XP-XCUT)22,32,32
    22 IF(TP-((XP-XZERO)/V1))23,24,24
    23 P=0.
        GO TO 81
    24 IF(TP-((XCUT-XZERO)/V1))25,26,26
    25 IF(V1*TP+XZERO)700,701,700
701 P=AKAY
    GO TO 81
700 P=AKAY/((V1*TP+XZERO)**GAMMA)
    GO TO 81
    26 P=AKAY/((XZERO+(V2*TP)+(1.-V2/V1)*(XCUT-XZERO))**GAMMA)
    GO TO 81
    32 IF(TP-(((XP-XCUT)/V2)+((XCUT-XZERO)/V1)))33,34,34
    33 P=0.
        GO TO 81
    34 P=AKAY/((XZERO+(V2*TP)+(1.-V2/V1)*(XCUT-XZERO))**GAMMA)
    GO TO 81
C   LOAD LINEARLY DECREASING TO LEFT OF LINE FOR ANY T
    41 IF(XP-XCUT)42,52,52
    42 IF(TP-((XP-XZERO)/V1))43,44,44
    43 P=0.
        GO TO 81
    44 IF(TP-((XCUT-XZERO)/V1))45,46,46
    45 IF(V1*TP+XZERO)702,703,702
703 P=AKAY
    GO TO 81
702 IF(TP-(+0.10000000E-05))760,760,761
760 P=(+0.20000000E+00)*AKAY/((XZERO+V1*TP)**GAMMA)
    GO TO 81
761 P=(((XP-XZERO)/(V1*TP))**4.)*AKAY/((XZERO+V1*TP)**GAMMA)
    GO TO 81
    46 IF(TP-(+0.10000000E-05))762,762,763
762 P=(+0.20000000E+00)*AKAY/((XZERO+(V2*TP)+(1.-V2/V1)*(XCUT-XZERO))*
1*GAMMA)
    GO TO 81
763 P=(((XP-XZERO)/((V2*TP)+(1.-V2/V1)*(XCUT-XZERO))**4.)*AKAY/((XZ
1ZERO+(V2*TP)+(1.-V2/V1)*(XCUT-XZERO))**GAMMA)
    GO TO 81
    52 IF(TP-(((XP-XCUT)/V2)+((XCUT-XZERO)/V1)))53,54,54
    53 P=0.
        GO TO 81
    54 IF(TP-(+0.10000000E-05))764,764,765
764 P=(+0.20000000E+00)*AKAY/((XZERO+(V2*TP)+(1.-V2/V1)*(XCUT-XZERO))*
1*GAMMA)
    GO TO 81
765 P=(((XP-XZERO)/((V2*TP)+(1.-V2/V1)*(XCUT-XZERO))**4.)*AKAY/((XZ

```



```

1ERC+(V2*TP)+(1.-V2/V1)*(XCUT-XZERO)**GAMMA)
GO TO 81
LOAD CONCENTRATED ALONG LINE
61 GO TO (63,62),NSTOP
62 P=0.
GO TO 81
63 IF(XP-XCUT)64,70,70
64 IF(TP-((XP-XZERO)/V1))65,66,66
65 P=0.
GO TO 81
66 IF(XP)705,706,705
706 P=AKAY
NSTOP=2
GO TO 81
705 P=AKAY/(XP**GAMMA)
NSTOP=2
GO TO 81
70 IF(TP-(((XP-XCUT)/V2)+((XCUT-XZERO)/V1)))71,72,72
71 P=0.
GO TO 81
72 P=AKAY/(XP**GAMMA)
NSTOP=2
GO TO 81
PRELIMINARY DEFINITIONS
100 X(1,1)=XZERO
T(1,1)=0.
U(1,1)=FUUI
UX(1,1)=FUUX1
UT(1,1)=FUUT1
V(1,1)=FUV1
VX(1,1)=FUVX1
VT(1,1)=FUVT1
W(1,1)=FUW1
WX(1,1)=FUWX1
WT(1,1)=FUWT1
IF(X(1,1))101,101,102
101 PL1(1,1)=AKAY1
PL2(1,1)=AKAY2
PL3(1,1)=AKAY3
S1=AZ1*UX(1,1)+AZ2*U(1,1)+AZ3*VX(1,1)+AZ4*V(1,1)+AZ5*WX(1,1)+AZ6*W
1(1,1)
S2=BZ1*UX(1,1)+BZ2*U(1,1)+BZ3*VX(1,1)+BZ4*V(1,1)+BZ5*WX(1,1)+BZ6*W
1(1,1)
S3=CZ1*UX(1,1)+CZ2*U(1,1)+CZ3*VX(1,1)+CZ4*V(1,1)+CZ5*WX(1,1)+CZ6*W
1(1,1)
GO TO 103
102 PL1(1,1)=AKAY1/(X(1,1)**GAMA1)
PL2(1,1)=AKAY2/(X(1,1)**GAMA2)
PL3(1,1)=AKAY3/(X(1,1)**GAMA3)
S1=AZ1*UX(1,1)+AZ2*U(1,1)+AZ3*VX(1,1)+AZ4*V(1,1)+AZ5*WX(1,1)+AZ6*W
1(1,1)+AZ7*U(1,1)/X(1,1)
S2=BZ1*UX(1,1)+BZ2*U(1,1)+BZ3*VX(1,1)+BZ4*V(1,1)+BZ5*WX(1,1)+BZ6*W
1(1,1)+BZ7*U(1,1)/X(1,1)
S3=CZ1*UX(1,1)+CZ2*U(1,1)+CZ3*VX(1,1)+CZ4*V(1,1)+CZ5*WX(1,1)+CZ6*W
1(1,1)+CZ7*U(1,1)/X(1,1)

```

```

103 PRINT 802,X(1,1),T(1,1),PL1(1,1),PL2(1,1),PL3(1,1),U(1,1),UX(1,1),
    1UT(1,1)
    PRINT 121,V(1,1),VX(1,1),VT(1,1),W(1,1),WX(1,1),WT(1,1),SI,S2,S3
    PRINT 8
    LI=2
    XLI=XLI
    NS1=1
    NS2=1
    NS3=1
    GO TO 200
C
REINDEXING OPERATIONS
110 LI=LI+1
    IF(LI-MZERO)111,111,9999
111 XLI=XLI
    KFF=2*LI-3
    DO 112 KFJ=1,KFF,1
    X(1,KFJ)=X(2,KFJ)
    T(1,KFJ)=T(2,KFJ)
    PL1(1,KFJ)=PL1(2,KFJ)
    PL2(1,KFJ)=PL2(2,KFJ)
    PL3(1,KFJ)=PL3(2,KFJ)
    U(1,KFJ)=U(2,KFJ)
    UX(1,KFJ)=UX(2,KFJ)
    UT(1,KFJ)=UT(2,KFJ)
    V(1,KFJ)=V(2,KFJ)
    VX(1,KFJ)=VX(2,KFJ)
    VT(1,KFJ)=VT(2,KFJ)
    W(1,KFJ)=W(2,KFJ)
    WX(1,KFJ)=WX(2,KFJ)
112 WT(1,KFJ)=WT(2,KFJ)
    NS1=1
    NS2=1
    NS3=1
C
INPUT POINT DEFINITIONS
200 X(2,1)=XZERO+2.*PINC*(XLI-1.)
    T(2,1)=0.
    XP=X(2,1)
    TP=T(2,1)
    MAMA=1
    IDIOT=1
    GO TO 20
201 GO TO (870,871,872),IDIOT
870 PL1(2,1)=P
    NS1=NSTOP
    IDIOT=2
    GO TO 20
871 PL2(2,1)=P
    NS2=NSTOP
    IDIOT=3
    GO TO 20
872 PL3(2,1)=P
    NS3=NSTOP
214 U(2,1)=FUU1
    UX(2,1)=FUUX1
    UT(2,1)=FUUT1

```

```

V(2,1)=FUV1
VX(2,1)=FUVX1
VT(2,1)=FUVT1
W(2,1)=FUW1
WX(2,1)=FUWX1
WT(2,1)=FUWT1
X(2,2)=X(2,1)-PINC
T(2,2)=PJNC/CEE1
XP=X(2,2)
TP=T(2,2)
MAMA=2
IDIOT=1
GO TO 20
202 GO TO (880,881,882),IDIOT
880 PL1(2,2)=P
NS1=NSTOP
IDIOT=2
GO TO 20
881 PL2(2,2)=P
NS2=NSTOP
IDIOT=3
GO TO 20
882 PL3(2,2)=P
NS3=NSTOP
X1=X(2,2)
X3=X(2,1)
X9=X(1,1)
U3=U(2,1)
UX3=UX(2,1)
UT3=UT(2,1)
V3=V(2,1)
VX3=VX(2,1)
VT3=VT(2,1)
W3=W(2,1)
WX3=WX(2,1)
WT3=WT(2,1)
U9=U(1,1)
UX9=UX(1,1)
UT9=UT(1,1)
V9=V(1,1)
VX9=VX(1,1)
VT9=VT(1,1)
W9=W(1,1)
WX9=WX(1,1)
WT9=WT(1,1)
X6=X9+2.*FAK1*PINC
X4=X3-2.*FAK1*PINC
U6=FUU1
UX6=FUUX1
UT6=FUUT1
V6=FUV1
VX6=FUVX1
VT6=FUVT1
W6=FUW1
WX6=FUWX1

```

```

WT6=FUWT1
U4=FUU1
UX4=FUUX1
UT4=FUUT1
V4=FUV1
VX4=FU VX1
VT4=FUVT1
W4=FUW1
WX4=FUWX1
WT4=FUWT1
FLD1=PL1(2,2)
FLD3=PL1(2,1)
FLD9=PL1(1,1)
GLD1=PL2(2,2)
GLD3=PL2(2,1)
GLD9=PL2(1,1)
HLD1=PL3(2,2)
HLD3=PL3(2,1)
HLD9=PL3(1,1)
HLD4=HLD3+FAK1*(HLD9-HLD3)
HLD6=HLD9+FAK1*(HLD3-HLD9)
GO TO 210

```

```

211 UX(2,2)=UU(1)
    UT(2,2)=UU(2)
    VX(2,2)=UU(3)
    VT(2,2)=UU(4)
    WX(2,2)=UU(5)
    WT(2,2)=UU(6)
    U(2,2)=U3+((UX(2,2)+UX3)/2.- (UT(2,2)+UT3)/(2.*CEE1))*DX13
    V(2,2)=V3+((VX(2,2)+VX3)/2.- (VT(2,2)+VT3)/(2.*CEE1))*DX13
    W(2,2)=W4+((WX(2,2)+WX4)/2.- (WT(2,2)+WT4)/(2.*CEE2))*DX14
    I=1

```

```

    XI=I
300 IF(2*LI-3-I)301,301,203
C   ORDINARY POINT DEFINITIONS
203 X(2,I+2)=XZERO+PINC*(2.*XLI-XI-3.)
    T(2,I+2)=(XI+1.)*PINC/CEE1
    XP=X(2,I+2)
    TP=T(2,I+2)
    MAMA=3
    IDIOT=1
    GO TO 20

```

```

204 GO TO (890,891,892),IDIOT

```

```

890 PL1(2,I+2)=P
    NS1=NSTOP
    IDIOT=2
    GO TO 20

```

```

891 PL2(2,I+2)=P
    NS2=NSTOP
    IDIOT=3
    GO TO 20

```

```

892 PL3(2,I+2)=P
    NS3=NSTOP
    X1=X(2,I+2)
    X3=X(2,I+1)

```

```

X9=X(1,I+1)
X6=X9+FAK2*PINC
X4=X3-FAK2*PINC
U3=U(2,I+1)
UX3=UX(2,I+1)
UT3=UT(2,I+1)
V3=V(2,I+1)
VX3=VX(2,I+1)
VT3=VT(2,I+1)
W3=W(2,I+1)
WX3=WX(2,I+1)
WT3=WT(2,I+1)
U9=U(1,I+1)
UX9=UX(1,I+1)
UT9=UT(1,I+1)
V9=V(1,I+1)
VX9=VX(1,I+1)
VT9=VT(1,I+1)
W9=W(1,I+1)
WX9=WX(1,I+1)
WT9=WT(1,I+1)
U4=U3+FAK2*(U(1,I)-U3)
UX4=UX3+FAK2*(UX(1,I)-UX3)
UT4=UT3+FAK2*(UT(1,I)-UT3)
V4=V3+FAK2*(V(1,I)-V3)
VX4=VX3+FAK2*(VX(1,I)-VX3)
VT4=VT3+FAK2*(VT(1,I)-VT3)
W4=W3+FAK2*(W(1,I)-W3)
WX4=WX3+FAK2*(WX(1,I)-WX3)
WT4=WT3+FAK2*(WT(1,I)-WT3)
U6=U9+FAK2*(U(1,I)-U9)
UX6=UX9+FAK2*(UX(1,I)-UX9)
UT6=UT9+FAK2*(UT(1,I)-UT9)
V6=V9+FAK2*(V(1,I)-V9)
VX6=VX9+FAK2*(VX(1,I)-VX9)
VT6=VT9+FAK2*(VT(1,I)-VT9)
W6=W9+FAK2*(W(1,I)-W9)
WX6=WX9+FAK2*(WX(1,I)-WX9)
WT6=WT9+FAK2*(WT(1,I)-WT9)
FLD1=PL1(2,I+2)
FLD3=PL1(2,I+1)
FLD9=PL1(1,I+1)
GLD1=PL2(2,I+2)
GLD3=PL2(2,I+1)
GLD9=PL2(1,I+1)
HLD1=PL3(2,I+2)
HLD3=PL3(2,I+1)
HLD9=PL3(1,I+1)
HLD4=HLD3+FAK2*(PL3(1,I)-HLD3)
HLD6=HLD9+FAK2*(PL3(1,I)-HLD9)
GO TO 210
212 UX(2,I+2)=UU(1)
    UT(2,I+2)=UU(2)
    VX(2,I+2)=UU(3)
    VT(2,I+2)=UU(4)

```

```

WX(2,I+2)=UU(5)
WT(2,I+2)=UU(6)
U(2,I+2)=U3+((UX(2,I+2)+UX3)/2.-(UT(2,I+2)+UT3)/(2.*CEE1))*DX13
V(2,I+2)=V3+((VX(2,I+2)+VX3)/2.-(VT(2,I+2)+VT3)/(2.*CEE1))*DX13
W(2,I+2)=W4+((WX(2,I+2)+WX4)/2.-(WT(2,I+2)+WT4)/(2.*CEE2))*DX14
I=I+1
XI=I
GO TO 300
C BOUNDARY POINT DEFINITIONS
301 X(2,I+2)=XZERO
T(2,I+2)=(XI+1.)*PINC/CEE1
XP=X(2,I+2)
TP=T(2,I+2)
MAMA=4
IDIOT=1
GO TO 20
302 GO TO (900,901,902),IDIOT
900 PL1(2,I+2)=P
NS1=NSTOP
IDIOT=2
GO TO 20
901 PL2(2,I+2)=P
NS2=NSTOP
IDIOT=3
GO TO 20
902 PL3(2,I+2)=P
NS3=NSTOP
X1=X(2,I+2)
X3=X(2,I+1)
X4=X3-FAK2*PINC
U3=U(2,I+1)
UX3=UX(2,I+1)
UT3=UT(2,I+1)
V3=V(2,I+1)
VX3=VX(2,I+1)
VT3=VT(2,I+1)
W3=W(2,I+1)
WX3=WX(2,I+1)
WT3=WT(2,I+1)
U4=U3+FAK2*(U(1,I)-U3)
UX4=UX3+FAK2*(UX(1,I)-UX3)
UT4=UT3+FAK2*(UT(1,I)-UT3)
V4=V3+FAK2*(V(1,I)-V3)
VX4=VX3+FAK2*(VX(1,I)-VX3)
VT4=VT3+FAK2*(VT(1,I)-VT3)
W4=W3+FAK2*(W(1,I)-W3)
WX4=WX3+FAK2*(WX(1,I)-WX3)
WT4=WT3+FAK2*(WT(1,I)-WT3)
FLD1=PL1(2,I+2)
FLD3=PL1(2,I+1)
GLD1=PL2(2,I+2)
GLD3=PL2(2,I+1)
HLD1=PL3(2,I+2)
HLD3=PL3(2,I+1)
HLD4=HLD3+FAK2*(PL3(1,I)-HLD3)

```

```

A1=CONSA
B1=CONSB
C1=CONSC
DX13=X1-X3
DX14=X1-X4
Y(2,1)=A11+A21*DX13/2.
Y(2,2)=A71-A21*DX13/(2.*CEE1)
Y(2,3)=A31+A41*DX13/2.
Y(2,4)=-A41*DX13/(2.*CEE1)
Y(2,5)=A51+A61*DX14/2.
Y(2,6)=-A61*DX14/(2.*CEE2)
Z(2)=A1-A21*DX13*(UX3-UT3/CEE1)/2.-A21*U3-A41*DX13*(VX3-VT3/CEE1)/
12.-A41*V3-A61*DX14*(WX4-WT4/CEE2)/2.-A61*W4
Y(4,1)=C11+C21*DX13/2.
Y(4,2)=-C21*DX13/(2.*CEE1)
Y(4,3)=C31+C41*DX13/2.
Y(4,4)=-C41*DX13/(2.*CEE1)
Y(4,5)=C51+C61*DX14/2.
Y(4,6)=C71-C61*DX14/(2.*CEE2)
Z(4)=C1-C21*DX13*(UX3-UT3/CEE1)/2.-C21*U3-C41*DX13*(VX3-VT3/CEE1)/
12.-C41*V3-C61*DX14*(WX4-WT4/CEE2)/2.-C61*W4
Y(5,1)=B11+B21*DX13/2.
Y(5,2)=-B21*DX13/(2.*CEE1)
Y(5,3)=B31+B41*DX13/2.
Y(5,4)=B71-B41*DX13/(2.*CEE1)
Y(5,5)=B51+B61*DX14/2.
Y(5,6)=-B61*DX14/(2.*CEE2)
Z(5)=B1-B21*DX13*(UX3-UT3/CEE1)/2.-B21*U3-B41*DX13*(VX3-VT3/CEE1)/
12.-B41*V3-B61*DX14*(WX4-WT4/CEE2)/2.-B61*W4
GO TO 215
213 UX(2,I+2)=UU(1)
UT(2,I+2)=UU(2)
VX(2,I+2)=UU(3)
VT(2,I+2)=UU(4)
WX(2,I+2)=UU(5)
WT(2,I+2)=UU(6)
U(2,I+2)=U3+((UX(2,I+2)+UX3)/2.-((UT(2,I+2)+UT3)/(2.*CEE1))*DX13
V(2,I+2)=V3+((VX(2,I+2)+VX3)/2.-((VT(2,I+2)+VT3)/(2.*CEE1))*DX13
W(2,I+2)=W4+((WX(2,I+2)+WX4)/2.-((WT(2,I+2)+WT4)/(2.*CEE2))*DX14
IF(X(2,I+2))220,221,220
221 S1=AZ1*UX(2,I+2)+AZ2*U(2,I+2)+AZ3*VX(2,I+2)+AZ4*V(2,I+2)+AZ5*WX(2,
1I+2)+AZ6*W(2,I+2)
S2=BZ1*UX(2,I+2)+BZ2*U(2,I+2)+BZ3*VX(2,I+2)+BZ4*V(2,I+2)+BZ5*WX(2,
1I+2)+BZ6*W(2,I+2)
S3=CZ1*UX(2,I+2)+CZ2*U(2,I+2)+CZ3*VX(2,I+2)+CZ4*V(2,I+2)+CZ5*WX(2,
1I+2)+CZ6*W(2,I+2)
GO TO 222
220 S1=AZ1*UX(2,I+2)+AZ2*U(2,I+2)+AZ3*VX(2,I+2)+AZ4*V(2,I+2)+AZ5*WX(2,
1I+2)+AZ6*W(2,I+2)+AZ7*U(2,I+2)/X(2,I+2)
S2=BZ1*UX(2,I+2)+BZ2*U(2,I+2)+BZ3*VX(2,I+2)+BZ4*V(2,I+2)+BZ5*WX(2,
1I+2)+BZ6*W(2,I+2)+BZ7*U(2,I+2)/X(2,I+2)
S3=CZ1*UX(2,I+2)+CZ2*U(2,I+2)+CZ3*VX(2,I+2)+CZ4*V(2,I+2)+CZ5*WX(2,
1I+2)+CZ6*W(2,I+2)+CZ7*U(2,I+2)/X(2,I+2)
222 PRINT 801,X(2,I+2),T(2,I+2),PL1(2,I+2),PL2(2,I+2),PL3(2,I+2),U(2,I
1+2),UX(2,I+2),UT(2,I+2)

```

```

PRINT 121,V(2,I+2),VX(2,I+2),VT(2,I+2),W(2,I+2),WX(2,I+2),WT(2,I+2
1),S1,S2,S3
PRINT 8
GO TO 110
81 GO TO (201,202,204,302),MAMA
210 DX13=X1-X3
DX14=X1-X4
DX16=X1-X6
DX19=X1-X9
F119=(CKF1/2.)*(+1./X1+1./X9)
F219=(CKF2/2.)*(1./X1**2+1./X9**2)+CKF2A
F319=CKF3
F419=CKF4
F519=CKF5
F619=CKF6
G119=CKG1
G219=CKG2
G319=CKG3
G419=CKG4
G519=CKG5
G619=CKG6
H116=CKH1
H216=(CKH2/2.)*(+1./X1+1./X6)
H316=CKH3
H416=CKH4
H516=(CKH5/2.)*(+1./X1+1./X6)
H616=CKH6
F719=(FLD1+FLD9)/2.
G719=(GLD1+GLD9)/2.
H716=(HLD1+HLD6)/2.
Y(2,1)=CEE1*(-1.+F119*DX19/2.+F219*DX19*DX13/4.)
Y(2,2)=1.-F219*DX19*DX13/4.
Y(2,3)=CEE1*(F319*DX19/2.+F419*DX19*DX13/4.)
Y(2,4)=-F419*DX19*DX13/4.
Y(2,5)=CEE1*(F519*DX19/2.+F619*DX19*DX14/4.)
Y(2,6)=-CEE1*F619*DX19*DX14/(4.*CEE2)
Z(2)=UT9-CEE1*UX9-(CEE1*DX19/2.)*(F119*UX9+F219*DX13*(UX3-UT3/CEE1
1)/2.+F219*(U3+U9)+F319*VX9+F419*DX13*(VX3-VT3/CEE1)/2.+F419*(V3+V9
2)+F519*WX9+F619*DX14*(WX4-WT4/CEE2)/2.+F619*(W4+W9)+2.*F719)
Y(4,1)=CEE1*(G119*DX19/2.+G219*DX19*DX13/4.)
Y(4,2)=-G219*DX19*DX13/4.
Y(4,3)=CEE1*(-1.+G319*DX19/2.+G419*DX19*DX13/4.)
Y(4,4)=1.-G419*DX19*DX13/4.
Y(4,5)=CEE1*(G519*DX19/2.+G619*DX19*DX14/4.)
Y(4,6)=-CEE1*DX19*DX14*G619/(4.*CEE2)
Z(4)=VT9-CEE1*VX9-(CEE1*DX19/2.)*(G119*UX9+G219*DX13*(UX3-UT3/CEE1
1)/2.+G219*(U3+U9)+G319*VX9+G419*DX13*(VX3-VT3/CEE1)/2.+G419*(V3+V9
2)+G519*WX9+G619*DX14*(WX4-WT4/CEE2)/2.+G619*(W4+W9)+2.*G719)
Y(5,1)=CEE2*(H116*DX16/2.+H216*DX16*DX13/4.)
Y(5,2)=-CEE2*DX16*DX13*H216/(4.*CEE1)
Y(5,3)=CEE2*(H316*DX16/2.+H416*DX16*DX13/4.)
Y(5,4)=-CEE2*DX16*DX13*H416/(4.*CEE1)
Y(5,5)=CEE2*(-1.+H516*DX16/2.+H616*DX16*DX14/4.)
Y(5,6)=1.-H616*DX16*DX14/4.
Z(5)=WT6-CEE2*WX6-(CEE2*DX16/2.)*(H116*UX6+H216*DX13*(UX3-UT3/CEE1

```



```

1)/2.+H216*(U3+U6)+H316*VX6+H416*DX13*(VX3-VT3/CEE1)/2.+H416*(V3+V6
2)+H516*WX6+H616*DX14*(WX4-WT4/CEE2)/2.+H616*(W4+W6)*2.*H716]
215 F113=(CKF1/2.)*(+1./X1+1./X3)
F213=(CKF2/2.)*(1./X1**2+1./X3**2)+CKF2A
F313=CKF3
F413=CKF4
F513=CKF5
F613=CKF6
G113=CKG1
G213=CKG2
G313=CKG3
G413=CKG4
G513=CKG5
G613=CKG6
H114=CKH1
H214=(CKH2/2.)*(+1./X1+1./X4)
H314=CKH3
H414=CKH4
H514=(CKH5/2.)*(+1./X1+1./X4)
H614=CKH6
F713=(FLD1+FLD3)/2.
G713=(GLD1+GLD3)/2.
H714=(HLD1+HLD4)/2.
Y(1,1)=CEE1*(1.-F113*DX13/2.-F213*DX13**2/4.)
Y(1,2)=1.+F213*DX13**2/4.
Y(1,3)=CEE1*(-F313*DX13/2.-F413*DX13**2/4.)
Y(1,4)=F413*DX13**2/4.
Y(1,5)=CEE1*(-F513*DX13/2.-F613*DX13*DX14/4.)
Y(1,6)=CEE1*DX13*DX14*F613/(4.*CEE2)
Z(1)=UT3+CEE1*UX3+CEE1*DX13*(F113*UX3/2.+F213*DX13*(UX3-UT3/CEE1)/
14.+F213*U3+F313*VX3/2.+F413*DX13*(VX3-VT3/CEE1)/4.+F413*V3+F513*WX
23/2.+F613*DX14*(WX4-WT4/CEE2)/4.+F613*(W4+W3)/2.+F713)
Y(3,1)=CEE1*(-G113*DX13/2.-G213*DX13**2/4.)
Y(3,2)=G213*DX13**2/4.
Y(3,3)=CEE1*(1.-G313*DX13/2.-G413*DX13**2/4.)
Y(3,4)=1.+G413*DX13**2/4.
Y(3,5)=CEE1*(-G513*DX13/2.-G613*DX13*DX14/4.)
Y(3,6)=CEE1*DX13*DX14*G613/(4.*CEE2)
Z(3)=VT3+CEE1*VX3+CEE1*DX13*(G113*UX3/2.+G213*DX13*(UX3-UT3/CEE1)/
14.+G213*U3+G313*VX3/2.+G413*DX13*(VX3-VT3/CEE1)/4.+G413*V3+G513*WX
23/2.+G613*DX14*(WX4-WT4/CEE2)/4.+G613*(W4+W3)/2.+G713)
Y(6,1)=CEE2*(-H114*DX14/2.-H214*DX14*DX13/4.)
Y(6,2)=CEE2*DX14*DX13*H214/(4.*CEE1)
Y(6,3)=CEE2*(-H314*DX14/2.-H414*DX14*DX13/4.)
Y(6,4)=CEE2*DX14*DX13*H414/(4.*CEE1)
Y(6,5)=CEE2*(1.-H514*DX14/2.-H614*DX14**2/4.)
Y(6,6)=1.+H614*DX14**2/4.
Z(6)=WT4+CEE2*WX4+CEE2*DX14*(H114*UX4/2.+H214*DX13*(UX3-UT3/CEE1)/
14.+H214*(U3+U4)/2.+H314*VX4/2.+H414*DX13*(VX3-VT3/CEE1)/4.+H414*(V
23+V4)/2.+H514*WX4/2.+H614*DX14*(WX4-WT4/CEE2)/4.*H614*W4+H714)
M=6
C THE MATRIX SUBROUTINE
5000 DU 5900 JJJ=1,M,1
IF(Y(JJJ,JJJ)-0.)5900,5850,5900
5850 PRINT 17

```

DISTRIBUTION

National Aeronautics and
Space Administration
Lewis Research Center
21000 Brookpark Road
Cleveland, Ohio 44135

Attn: Contracting Officer, M.S. 500-210 (1)
Liquid Rocket Technology Branch,
M.S. 500-209 (8)
Technology Utilization Office,
M.S. 3-16 (1)
Technical Report Control Office,
M.S. 5-5 (1)
AFSC Liaison Office, M.S. 4-1 (2)
Library, M.S. 60-3 (2)
Office of R&QA, M.S. 500-203 (1)
F. S. Stepka, M.S. 49-1 (1)
J. F. Mondt, M.S. 500-309 (1)
Robert Johns, M.S. 49-1 (1)

National Aeronautics and
Space Administration
Langley Research Center
Langley Station
Hampton, Virginia 23365

Attn: Mrs. E. R. Gilman, Librarian (1)
Mr. D. Davis, Jr. (1)
Mr. Richard Heldenfels (1)
Mr. William Kinard (1)
Mr. Edwin Kruszewski, M.S. 188 (1)

National Aeronautics and
Space Administration
Ames Research Center
Moffett Field, California

Attn: C. Robert Nysmith (1)
James Summers (1)
Library (2)

National Aeronautics and
Space Administration
George C. Marshall Space Flight Center
Huntsville, Alabama

Attn: Tech. Documents Library (4)
Research Projects Div. (M-RP-R) (1)
James W. Carter, Future Projects
Office, MFPO (1)

National Aeronautics and
Space Administration Headquarters
Washington, D. C. 20546

Attn: MLPL (6)
Melvin Rosche; Code RV-2 (1)

National Aeronautics and
Space Administration
Manned Spacecraft Center
Houston, Texas

Attn: Library (2)

Jet Propulsion Laboratory
4800 Oak Drive
Pasadena 2, California

Attn: Earl E. Newham, Reports Group (2)
Dr. V. Jaffe (1)

National Aeronautics and
Space Administration
Goddard Space Flight Center
Greenbelt, Maryland

Attn: Code 250 (1)

Wright Patterson Air Force Base
Ohio

Attn: Lt. Lloyd Hedgepeth, ASRMFP-1 (1)
W. P. Conrardy, Chief,
Applications Lab-
Materials Control (1)
Commander, Air Tech. Intelli-
gence Center
Attn: AFOIN-4B1A (2)

Scientific and Technical Information
Facility
P. O. Box 5700
Bethesda, Maryland

Attn: NASA Representative
(S-AK/RKT) (6)

University of California
Los Alamos Scientific Laboratory
P. O. Box 1663
Los Alamos, New Mexico (1)

```

PRINT 5960
GO TO 9999
5900 CONTINUE
N=M-1
DO 5200 NN=1,N,1
NNN=NN+1
DO 5100 JJ=NNN,M,1
FRAC=-Y(JJ,NN)/Y(NN,NN)
DO 5050 KK=NN,M,1
5050 Y(JJ,KK)=FRAC*Y(NN,KK)+Y(JJ,KK)
5100 Z(JJ)=FRAC*Z(NN)+Z(JJ)
5200 CONTINUE
DO 5500 NN=1,N,1
NNN=M-NN
JJ=NNN+1
DO 5400 KK=1,NNN,1
5400 Z(KK)=-Z(JJ)*(Y(KK,JJ)/Y(JJ,JJ))+Z(KK)
5500 CONTINUE
DO 5600 KKK=1,M,1
5600 UU(KKK)=Z(KKK)/Y(KKK,KKK)
C SOLUTION CONTROL
GO TO (214,211,212,213),MAMA
9999 CONTINUE
STOP
END

```

Prof. Pei Chi Chou Dept. Mechanical Engineering Drexel Institute of Technology Philadelphia, Pennsylvania 19104	(1)	Boeing Company Seattle 24, Washington	(1)
New York University College of Engineering Research Division University Heights New York 53, New York		Chance Vought Corporation Library Box 5907 Dallas 22, Texas	(1)
Attn: Dr. Paul F. Winternitz	(1)	Chrysler Corporation P. O. Box 26018 New Orleans 26, La.	(1)
Harvard College Observatory Cambridge, Massachusetts		Attn: Elayne M. Brower-AEB-2761	(1)
Attn: Prof. F. L. Whipple	(1)	Douglas Aircraft Corporation 3000 Ocean Park Blvd. Santa Monica, California	
Cornell Aeronautical Laboratory, Inc. Buffalo, New York		Attn: G. W. Ferguson H. H. Dixon	(1) (1)
Attn: Dr. William Rae	(1)	Fundamental Methods Associates 31 Union Square West New York 3, New York	
Stanford Research Institute Menlo Park, California		Attn: Dr. Carl Klahr	(1)
Attn: Mr. P. R. Gillette	(1)	General Dynamics/Convair P. O. Box 1128 San Diego 12, California	
Arthur D. Little Inc. Cambridge, Massachusetts		Attn: Library & Information Service (128-00)	(2)
Attn: Dr. J. M. Bonneville	(1)	General Electric Valley Forge Space Tech. Center P. O. Box 8555 Philadelphia 1, Pennsylvania	
Research and Technology Division, AFSC Bolling Field Washington, D. C.		Attn: T. D. Riney - TEMO J. F. Heyda - TEMO	(1) (1)
Attn: J. W. Minette E. A. Kritzer	(1) (1)	General Motors Defense Research Labs. Santa Barbara, California	
Aerojet-General Corporation Von Karman Center, Azusa, California 91703		Attn: C. J. Maiden	(1)
Attn: J.F. Cullinane-Downey Plant	(1)	Grumman Aircraft Engineering Corporation Bethpage, Long Island, New York	
Avco Corporation Wilmington, Massachusetts 01887		Attn: Library John Tlasmati	(1)
Attn: Robert R. McMath - RAD	(1)		
Battelle Memorial Institute 505 King Avenue Columbus, Ohio			
Attn: R.E. Bowman - Rad. Effects Information Center	(1)		

IIT Research Institute
10 West 35 Street
Chicago 16, Illinois

Attn: Dr. R. H. Cornish (1)

Lockheed Missiles and Space Company
Palo Alto, California

Attn: P. E. Sandorff (1)

The Martin Company
Science Technology Library
Mail Stop 398
Baltimore 3, Maryland

(1)

North American Aviation
Space & Information Division
Downey, California

Attn: Allan J. Richardson, D/192 GB83 (1)

Northrop Space Laboratories
3401 West Broadway
Hawthorne, California 90250

Attn: R. D. Johnson,
Space Materials Laboratory (1)

Republic Aviation Corporation
Farmingdale, Long Island, New York

Attn: K. Singer, Space Systems
Structures (1)

TRW Systems
Physical Research and Analysis Section
P. O. 95001
Los Angeles 45, California

(1)

University of Denver
Denver Research Institute
University Park
Denver, Colorado 80210

Attn: Rodney F. Recht,
Mechanics Division (1)

Utah Research and Development
2175 South 3270 West
Salt Lake City, Utah

Attn: Boyd Baugh (1)

Computing Devices of Canada Limited
P. O. Box 508
Ottawa 4, Canada

Attn: Dr. G. P. T. Wilenius (1)

Wright-Patterson Air Force Base
Ohio

Attn: Commander, Air Tech.
Intelligence Center
Attn: AFLIN-4BIA (1)
Lt. Lloyd Hedgepeth, ASRMFP-1 (1)
F. Sachleh (1)

Naval Research Laboratory
Washington, D. C.

Attn: Walter W. Atkins (1)
Mario A. Persechino (1)

Naval Ordnance Laboratory
Maryland

Attn: Arnold E. Seigel (1)

Naval Ordnance Laboratory
Corona, California

Attn: Roy L. Nicholi (1)
F. E. Winters, Jr. (1)

Space Systems Division, AFSC

Attn: Major R. L. Hayford (1)

Ballistic Research Laboratory
Aberdeen, Maryland

Attn: Stanley Taylor (1)
Robert J. Eichelberger (1)

A. F. Cambridge Research Laboratory
Hanscom Field, Mass.

Attn: Robert K. Soberman (1)

Aero-Space Corporation
El Segundo, California

Attn: Robert Cooper (1)
Verne C. Frost (1)
Robert Herndon (1)
J. McClelland (1)
Milton Weiss (1)

Aerospace Corporation
San Bernardino, California

Attn: Rene B. Mortensen (1)
D. B. Singer (1)

University of Toronto
Toronto, Canada

Attn: I. I. Glass (1)

Pennsylvania State University
University Park, Pennsylvania

Attn: Norman Davids (1)

Sandia Corporation
Albuquerque, New Mexico

Attn: Walter Herrmann (1)

ARO
Tullahoma, Tenn.

Attn: Julius Lukasiewicz (1)

Space Research Center
McGill University
892 Sherbrooke Street, West
Montreal, Quebec
Canada

Attn: G. V. Bull (3)

DOCUMENT CONTROL DATA - R&D

(Security classification of title, body of abstract and indexing annotation must be entered when the overall report is classified)

1. ORIGINATING ACTIVITY (Corporate author) DREXEL INSTITUTE OF TECHNOLOGY Phila. Pa. 19104		2a. REPORT SECURITY CLASSIFICATION Unclassified	
		2b. GROUP N/A	
3. REPORT TITLE ANALYTICAL STUDY OF THE FRACTURE OF LIQUID-FILLED TANKS IMPACTED BY HYPERVELOCITY PARTICLES			
4. DESCRIPTIVE NOTES (Type of report and inclusive dates) Technical Research Report			
5. AUTHOR(S) (Last name, first name, initial) Chou, P.C. Schaller, R. Hoburg, J.			
6. REPORT DATE		7a. TOTAL NO. OF PAGES	7b. NO. OF REFS 21
8a. CONTRACT OR GRANT NO. NsG-270		9a. ORIGINATOR'S REPORT NUMBER(S) 160-9	
b. PROJECT NO.		9b. OTHER REPORT NO(S) (Any other numbers that may be assigned this report) NASA CR-72169	
c.			
d.			
10. AVAILABILITY/LIMITATION NOTICES Distribution of this report is unlimited			
11. SUPPLEMENTARY NOTES		12. SPONSORING MILITARY ACTIVITY NASA, Lewis Research Center	
13. ABSTRACT The problem of the fracture of liquid-fuel tank walls due to hypervelocity particle impact is investigated. A semi-empirical formula is used for the shock wave generated by impact in water. The numerical method of characteristics is adopted for the calculation of stress waves in the tank wall. Values of threshold impact kinetic energy; defined as the projectile energy above which fracture will occur, for a few wall thickness and materials are determined.			

14. KEY WORDS	LINK A		LINK B		LINK C	
	ROLE	WT	ROLE	WT	ROLE	WT

INSTRUCTIONS

1. ORIGINATING ACTIVITY: Enter the name and address of the contractor, subcontractor, grantee, Department of Defense activity or other organization (*corporate author*) issuing the report.

2a. REPORT SECURITY CLASSIFICATION: Enter the overall security classification of the report. Indicate whether "Restricted Data" is included. Marking is to be in accordance with appropriate security regulations.

2b. GROUP: Automatic downgrading is specified in DoD Directive 5200.10 and Armed Forces Industrial Manual. Enter the group number. Also, when applicable, show that optional markings have been used for Group 3 and Group 4 as authorized.

3. REPORT TITLE: Enter the complete report title in all capital letters. Titles in all cases should be unclassified. If a meaningful title cannot be selected without classification, show title classification in all capitals in parenthesis immediately following the title.

4. DESCRIPTIVE NOTES: If appropriate, enter the type of report, e.g., interim, progress, summary, annual, or final. Give the inclusive dates when a specific reporting period is covered.

5. AUTHOR(S): Enter the name(s) of author(s) as shown on or in the report. Enter last name, first name, middle initial. If military, show rank and branch of service. The name of the principal author is an absolute minimum requirement.

6. REPORT DATE: Enter the date of the report as day, month, year, or month, year. If more than one date appears on the report, use date of publication.

7a. TOTAL NUMBER OF PAGES: The total page count should follow normal pagination procedures, i.e., enter the number of pages containing information.

7b. NUMBER OF REFERENCES: Enter the total number of references cited in the report.

8a. CONTRACT OR GRANT NUMBER: If appropriate, enter the applicable number of the contract or grant under which the report was written.

8b, 8c, & 8d. PROJECT NUMBER: Enter the appropriate military department identification, such as project number, subproject number, system numbers, task number, etc.

9a. ORIGINATOR'S REPORT NUMBER(S): Enter the official report number by which the document will be identified and controlled by the originating activity. This number must be unique to this report.

9b. OTHER REPORT NUMBER(S): If the report has been assigned any other report numbers (*either by the originator or by the sponsor*), also enter this number(s).

10. AVAILABILITY/LIMITATION NOTICES: Enter any limitations on further dissemination of the report, other than those imposed by security classification, using standard statements such as:

- (1) "Qualified requesters may obtain copies of this report from DDC."
- (2) "Foreign announcement and dissemination of this report by DDC is not authorized."
- (3) "U. S. Government agencies may obtain copies of this report directly from DDC. Other qualified DDC users shall request through _____."
- (4) "U. S. military agencies may obtain copies of this report directly from DDC. Other qualified users shall request through _____."
- (5) "All distribution of this report is controlled. Qualified DDC users shall request through _____."

If the report has been furnished to the Office of Technical Services, Department of Commerce, for sale to the public, indicate this fact and enter the price, if known.

11. SUPPLEMENTARY NOTES: Use for additional explanatory notes.

12. SPONSORING MILITARY ACTIVITY: Enter the name of the departmental project office or laboratory sponsoring (*paying for*) the research and development. Include address.

13. ABSTRACT: Enter an abstract giving a brief and factual summary of the document indicative of the report, even though it may also appear elsewhere in the body of the technical report. If additional space is required, a continuation sheet shall be attached.

It is highly desirable that the abstract of classified reports be unclassified. Each paragraph of the abstract shall end with an indication of the military security classification of the information in the paragraph, represented as (TS), (S), (C), or (U).

There is no limitation on the length of the abstract. However, the suggested length is from 150 to 225 words.

14. KEY WORDS: Key words are technically meaningful terms or short phrases that characterize a report and may be used as index entries for cataloging the report. Key words must be selected so that no security classification is required. Identifiers, such as equipment model designation, trade name, military project code name, geographic location, may be used as key words but will be followed by an indication of technical context. The assignment of links, rules, and weights is optional.